DEVELOPMENT OF A THREE-AXIS LONG-PERIOD SEISMOGRAPH

ANNUAL REPORT

prepared for

AIR FORCE OFFICE OF SCIENTIFIC RESEARCH

ARLINGTON, VIRGINIA

Arthur D. Little, Inc.

ANNUAL REPORT

Reporting Date: 31 May 1968

DEVELOPMENT OF A THREE-AXIS LONG-PERIOD SEISMOGRAPH

ARPA Order No. 1029
Program Code No. 7F10

Contractor: Arthur D. Little, Inc.
Research and Development Division
15 Acorn Park
Cambridge, Massachusetts 02140

Date of Contract: 1 June 1967

[redacted]

Contract No.: F44620-67-C-0107

[redacted]

Principal Investigator: Ivan Simon, (617) 864-5770

Report Co-authors: M. L. Cohen, A. G. Emslie, R. K. McConnell, C. R. Smallman, R. S. Stone, P. F. Strong

C-69429

Arthur D. Little, Inc.

TABLE OF CONTENTS

LIST OF FIGURES

LIST OF FIGURES (Continued)

ABSTRACT

Development of a three-component long-period borehole seismometer of small diameter (5 1/2 in. O.D.) is described. The feasibility of the magnetic suspension principle has been demonstrated and several instruments have been constructed and tested in the laboratory.

I. INTRODUCTION

The present report covers the development of a three-axis long-period seismograph suitable for operation in 5- to 6-inch diameter boreholes. This program relates to ARPA's interest in further improvements of the capability to discriminate between natural and man-made teleseismic events of small magnitude (m = 3.5 to 5.5 for the body waves) based on the comparison of their apparent short-period and long-period magnitudes.

While the detection capability provided by the existing short-period borehole seismometers appears to be quite satisfactory, the capability of the long-period instruments cannot be fully utilized as long as they are installed in shallow vaults. When operated near the surface, the long-period, horizontal-component instruments are limited in their performance by the high level of ground noise at low frequencies. This type of noise is believed to result from random motions of ground blocks generated locally by environmental factors such as barometric pressure, wind, and temperature. In order to avoid this situation, the long-period instruments should be placed in deep boreholes (500 feet or deeper) at selected sites. Conventional long-period seismometers are not suited for installation in boreholes because of their large size. Even the recently developed borehole seismometers require boreholes of large diameters (11 to 12 in. I.D.) which tend to be expensive.

Development of the magnetic suspension at Arthur D. Little, Inc. and its subsequent applications in tiltmeters and other instruments led

us to propose the development of borehole seismometers small enough to fit in boreholes of 5- to 6-inch diameter.

Practical feasibility of such instruments has been demonstrated during this year's effort and the instruments have successfully undergone numerous laboratory tests.

Even though it was not anticipated that instruments of this type would necessarily have overall performance superior to that of high quality station-type instruments which are in existence, it appears that the performance of the instruments will be high enough to permit ground-noise limited operation in the long period passband at most of the typical sites.

II. SEISMOLOGICAL BACKGROUND FOR THE INSTRUMENT SPECIFICATIONS

The present program relates to ARPA's interest in further improving the capability to descriminate between small natural and man-made teleseismic events (m $\gtrsim$ 3.5 to 5.5) by comparison of their magnitudes at short and long periods.

While arrays using existing short period borehole seismometers are able to detect events in this range, long period horizontal component instruments are usually limited in their performance by low frequency tilting, caused by local environmental factors such as barometric pressure changes, wind and temperature changes. Much of this tilt noise, particularly that related to temperature fluctuations can be significantly reduced by careful site selection and by placing the long period instruments in boreholes several hundred feet deep. As the cost of borehole preparation climbs rapidly with increasing diameter, practical long-period instruments should combine ruggedness, reliability and small (6 inches or less) diameter.

The operating parameters of the instrument are basically determined by the comparative power distribution in the spectra of the signals which one is trying to detect and of the microseismic ground noise. The signals being sought are primarily surface waves of the Love and Rayleigh types generated by teleseismic events. Because of the velocity characteristics of the earth's crust and upper mantle surface waves from teleseismic events are highly dispersed, wave trains of many minutes

duration whose energy is concentrated predominantly in a frequency band between approximately 0.025 and 0.10 Hz (10 to 40 sec.). Below 0.01 Hz, the energy of the signal becomes insignificant except for the largest natural earthquakes while the energy of the ground noise begins to rise rapidly from its minimum, around 0.02 to 0.03 Hz.

Larger teleseisms have most of their surface wave energy concentrated near the microseismic noise minimum, but for smaller events this energy may be shifted towards somewhat higher frequencies. We show in Figure 1 some representative data collected from various sources illustrating typical microseismic power spectra in the range 0.01 to 1.0 Hz. While it is customary to discuss microseismic noise in terms of displacement, for consistency with the discussion in following parts of this report we have expressed the data in terms of mean square acceleration $(cm/sec^2)^2$ per Hz. As suggested by the diagram, the typical microseismic noise spectrum varies greatly from place to place and may range over several orders of magnitude depending on meteorological conditions, geological conditions and distance from the ocean.

Although most of the noise spectra shown in Figure 1 are based on vertical component instruments, on the high frequency side of the microseismic minimum the magnitudes of the horizontal and vertical noise spectra are comparable and for the purposes of the present discussion, little distinction need be made between them. At long periods, however, the similarity is not so pronounced. Long period horizontal seismometers are notoriously sensitive to tilts whether they are due to wind loading, thermal fluctuations, barometric pressure changes, or earth tides.

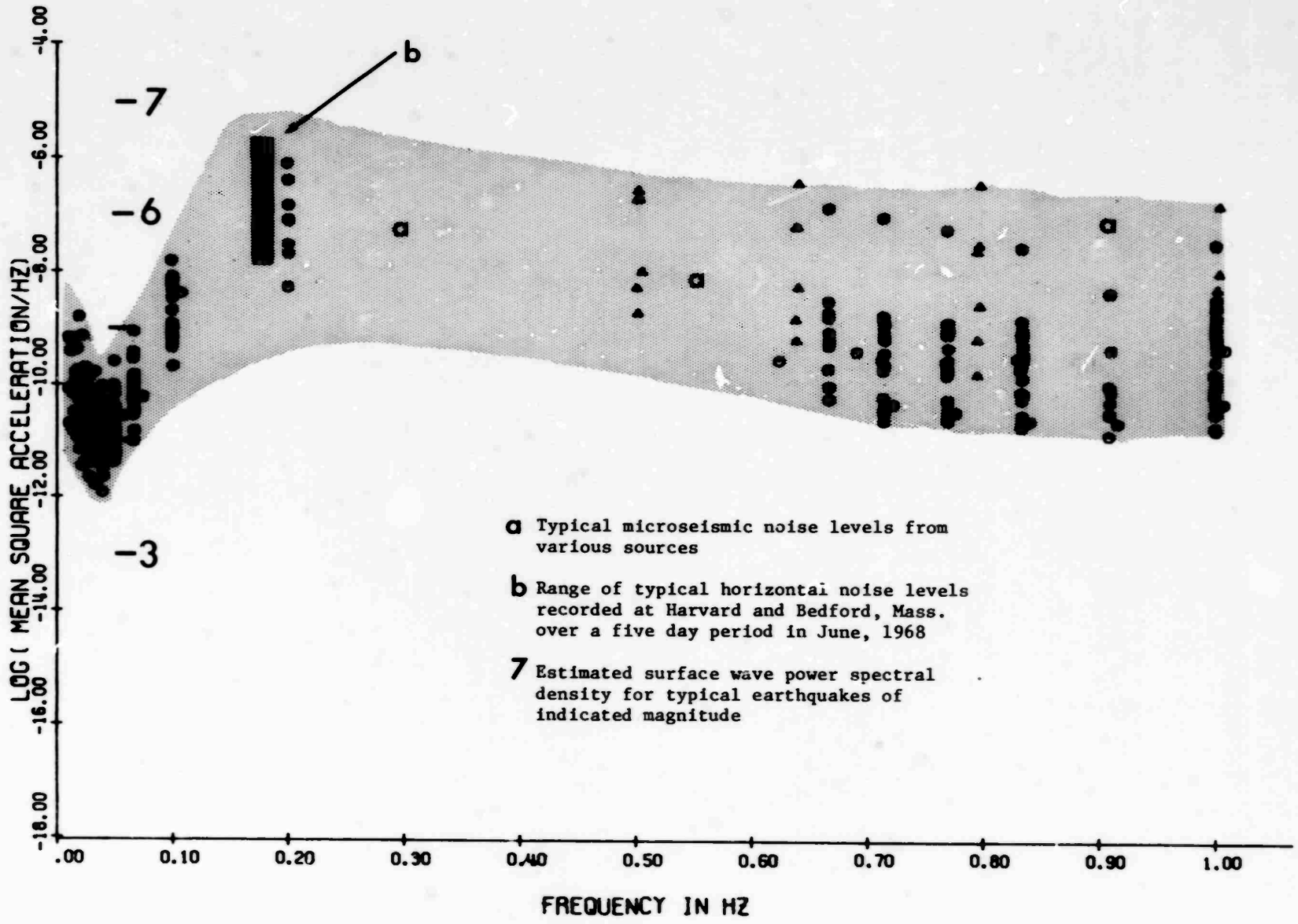

FIGURE 1 COMPARISON OF ESTIMATED ACCELERATION POWER SPECTRA OF SURFACE WAVES FROM NATURAL TELESEISMIC EVENTS WITH MICROSEISMIC NOISE ESTIMATES COMPILED FROM VARIOUS SOURCES

These tilts result in signals which by themselves are indistinguishable from long period surface waves and their frequently large amplitude imposes stringent requirements on the linearity and dynamic range of the instrument. Although the relative proportions of long period noise contributed by each of the various sources is still a subject of considerable research, it is clear, both from our own work and that of others, that extremely small temperature fluctuations on the pier, or on the instrument can produce major effects. By placing the instruments in deep boreholes these temperature effects can be minimized and thus one can expect to remove a large portion of the locally induced noise leaving only the signal caused by propagating seismic waves.

A more quantitative comparison of the relative amplitudes of the teleseismic signals and noise is shown in Figure 1 where we also plot the signal level from earthquakes of various magnitudes M, as observed on local test piers. The values shown were obtained by first estimating the spectra for events of surface wave magnitude around 7, and then scaling to smaller magnitudes assuming that the shape of the spectrum has not changed in the region of interest. From this diagram it is clear that except for the most ideal sites most of the surface wave signals from events in the range from 3.5 to 5.5 will be comparable to or smaller than the microseismic noise, from which they must be separated by various signal processing techniques. We also show in Figure 1 some preliminary data on the microseismic noise at two local sites (Harvard and Bedford, Massachusetts) which we have been considering for use as test piers. At both these sites the 6-second microseismic noise is relatively high, typical of locations near the seacoast.

In view of the above discussion it is possible to reach conclusions about the operating characteristics the instrument should have. 0.01 Hz (100 sec. period) can be taken as a lower bound for the operating frequency band of the seismometer. At the upper frequency end the signal tends to overlap the large microseismic noise peak located typically between 0.15 and 0.2 Hz. Even though the ground noise power density at the peak may be 4 to 6 orders of magnitude greater than at the minimum, it is desirable (when array data processing is considered) that the instrument itself have the capability of handling this large dynamic range over the entire frequency band including the microseismic peak. Accordingly, the upper end of the operating frequency band may be placed somewhere around 0.2 to 1 Hz.

The most desirable "center frequency" of the operating frequency band, usually associated with the natural frequency of the seismometer, is determined by the spectral distribution of the signal and the ground noise; but in practice is limited by the requirements of instrument design and its mode of operation. We may estimate that the center frequency will be most likely between 0.02 to 0.04 Hz.

The absolute sensitivity of the seismometer may be specified in reference to the minimum signal expected and the level of the microseismic ground noise at the operating location. As has been pointed out above, this level is, of course, highly variable from place to place and depends on both seasonal and occasional meteorological conditions. Depending on the kind of intended data processing, additional margin between ground noise and instrument noise might be needed. However, as

a first estimate it appears that to detect surface waves from events of magnitude M_s = 3.5 to 5.5, the instrument should be able to detect signals of average spectral density of 10^{-12} $(cm/sec^2)^2/Hz$ over a bandwidth of 0.02 to 0.04 Hz. This is approximately the level of the lowest microseismic noise reported, and 30 db below that of the highest values.

Based on these considerations we may summarize the design goals of the present program in the form of a tentative set of specifications as follows:

Type of Instrument:	Three-component, 6 in. borehole seismometer with two (identical) horizontal component modules and one vertical component module.
Operating Frequency Band:	0.01 to 1.0 Hz (1 to 100 sec. period).
Ultimate Sensitivity:	Approximately 10 mμ rms ground displacement at frequencies between .02 to .04 Hz.
Type of Suspension:	Magnetic.
Weight of Seismic Mass:	Approximately 1 and 10 gms for the horizontal and vertical modules, respectively.
Damping:	Electromagnetic
Readout:	Displacement type.
Mode of Operation:	Feedback.
Dynamic Range:	Approximately 80 db.

III. HORIZONTAL SEISMOMETER

A. OPERATING PRINCIPLES

1. Diamagnetic Suspension.

The horizontal seismometer employs the principle of diamagnetic levitation to suspend a seismic mass in a suitably shaped magnetic field so that the mass is constrained to move in the direction of a single horizontal axis. The period of the pendulous motion of the mass is determined essentially by the depth of its potential minimum due to the configuration of the magnetic field. In this sense the elastic force of a spring or the gravity force acting on a pendulum is replaced by a magnetic field force. The suspension is inherently free of any external (Coulomb) or internal (anelastic) friction. However, velocity-proportional eddy current damping can be introduced at will.

The field configuration utilized in the horizontal diamagnetic seismograph is characterized by a strong gradient pointing upwards, intermediate gradient in the lateral horizontal directions, and very weak gradient along the sensitive axis longitudinal horizontal directions. The vertical gradient must have a value given by the equation

$$\left| \chi v H_y \frac{\partial H_y}{\partial y} \right| = mg \qquad (1)$$

which expresses the equality of the magnetic lifting force and the weight of the seismic mass (condition of levitation); here χ represents the susceptibility of the diamagnetic seismic mass, v the volume of the mass,

H_y the vertical component of the field, and mg the weight of the seismic mass. Since χ has a small numerical value (typically about -6×10^{-6} in cgs units for graphite, which is the best available material), the value of $H_y(\partial H_y/\partial y)$ must be very large, typically of the order of 10^8 Oe^2/cm. Nevertheless, gradients of this magnitude can be readily produced with commercially available permanent magnets in working gaps as large as 0.1 inch.

The lateral gradients are obtained by shaping the field in a multipole geometry, or, in the simplest case, by an edge-and-groove arrangement of magnet polepieces as indicated schematically below:

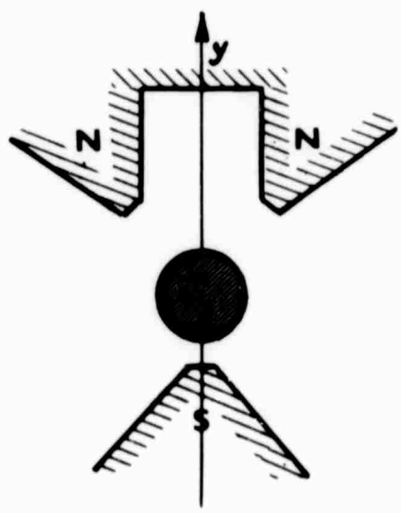

Fig. 2. Polepiece configuration used for magnetic suspension of the diamagnetic seismic mass (cross section).

The sensitive (horizontal) axis is perpendicular to the plane of this diagram and the suspended seismic mass (circular in cross section) extends some forty to fifty diameters along its length. The weak longitudinal gradient along the horizontal axis is obtained by making the axial (z) component of the field initially as near zero as possible and then introducing a small perturbation by judicious application of flux shunts or disposition of magnets along the polepieces.

We shall outline now how the physical parameters of the suspension can be derived from the properties of the magnetic field. The field configuration according to Figure 2 is not readily describable in mathematical form. However, fields of the multipole symmetry which are configurationally similar to it can be derived from a magnetostatic potential of the form

$$\Omega = C\, J_n(kr) \sin n\theta \cosh(kz). \qquad (2)$$

This potential satisfies Laplace's equation $\nabla^2\Omega = 0$ and therefore describes a physically realizable field. Here r is the radial coordinate, θ the azimuth, and n an integer which defines the periodicity of the field about the z-axis (n = number of pole-pairs around the circumference); $J_n(kr)$ is the n^{th}-order Bessel function of the first kind, and k is a constant which determines the depth of the potential well in the z direction. The field components, H_r, H_θ are derived from equation (2) as $-\partial\Omega/\partial r$ and $-r^{-1}\,\partial\Omega/\partial\theta$. For small values of kr and kz, equation (2) has the approximate form

$$\Omega = A\, r^n \sin n\theta \left(1 + \tfrac{1}{2} k^2 z^2\right) \qquad (3)$$

The constant A can be expressed in terms of the maximum field strength H_m at r = b (the distance of the pole tips from the axis):

$$A = \frac{1}{n} H_m b^{(1-n)}.$$

The potential energy V of the diamagnetic body (a cylinder of radius a and susceptibility X) suspended in the field is determined by the integral of H^2 over the volume of the cylinder.

The potential energy is

$$V = \frac{1}{2} |X| \int_{cyl.} \left[n^2 A^2 r^{2n-2} \left(1 + \frac{1}{2} k^2 z^2 \right) + k^4 r^{2n} z^2 \sin^{2n} \theta \right] dv \qquad (4)$$

where dv is an element of volume of the cylinder. On carrying out the integration in Eq. (4) for the case where the cylinder is displaced, an amount h radially and z longitudinally, one can calculate the longitudinal spring constant K from the formula

$$K = \frac{\partial^2 V}{\partial z^2} \qquad (5)$$

One can show that for n = 2, K has the form:

$$K = \pi \ell (a/b)^2 |X| H_m^2 \left(h^2 + \frac{1}{2} a^2 \right) k^2. \qquad (6)$$

Here ℓ is the length of the suspended cylinder and H_m is the maximum field at the polepiece tips (r = b). The restoring force is seen to be determined by the magnitude of k, but is also dependent on H_m. Therefore, if the period of the instrument is to remain constant, the product $|X| H_m^2$ should not vary with time, temperature, external fields, etc.

2. Readout System and Instrument Noise.

The readout system used in the present series of experimental seismometers is of the electrooptical type. The quantity sensed by the readout is the displacement of the seismic mass relative to the frame of the instrument. Because of the proportionality of the displacement to the inertial force acting on the seismic mass, the output of the readout is proportional to the frame (and ground) acceleration. This type of readout is particularly well suited for the diamagnetic seismometer because it requires no bodily contact between the suspended seismic mass and the frame; furthermore, the optical readout exerts no forces on the seismic mass in the direction of the sensitive axis.

The ultimate limit of sensitivity is determined by the "noise" inherent to the instrument. One source of noise is the photodetector used in the optical readout. In the semiconducting photodetectors this noise results from the statistical fluctuations in the rate of generation and recombination of the current carriers. Unlike Johnson noise its frequency distribution is not "white," and its magnitude depends on the current passing through the device. The other source of noise is that resulting from the Brownian motion of the suspended mass. While this noise is negligible in conventional seismometers employing masses of several kilograms, it becomes significant in the present seismometer in which the seismic mass is of the order of one gram.

It can be shown that the r.m.s. value of the "noise displacement" (z_n) of a mass m restrained by a force constant K, when observed

over a frequency range from 0 to ∞ is given by an expression

$$(z_n)_{rms} = \frac{1}{\omega_o}\sqrt{\frac{k_b T}{m}} \tag{7}$$

where $\omega_o = (K/m)^{\frac{1}{2}}$ is the undamped natural period of the seismometer and $k_b = 1.38 \times 10^{-16}$ erg sec deg^{-1} is the Boltzmann constant. In order to obtain the r.m.s. value of the noise displacement observable in a given bandwidth, it is necessary to consider the frequency response of the seismometer.

For a pendulous system of a mass m, natural frequency ω_o and damping coefficient α, the mean square noise between the frequencies ω_1 and ω_2 is

$$z_n^2 = \frac{4kT\alpha}{\pi m\omega_o^2}\int_{w_1}^{w_2} \frac{dw}{1 + 2w^2}\frac{}{(2\alpha^2 - 1) + w^4} \tag{8}$$

$w = \omega/\omega_o$ is the dimensionless frequency.

This result can be derived on the basis of an equivalent LCR circuit in which the inductance represents the mass, the capacitance, the restoring force and the resistance, the damping. The Johnson noise in the damping resistance generates a charge fluctuation in the capacitance which corresponds to the noise displacement. This treatment yields a result identical with that obtained from the kinetic theory when the integral is taken between the limits 0 to ∞. Eq. (8) is therefore a generalization of Eq. (7).

Evaluation of Eq. (8) for a seismic mass 0.7 gms under typical operating conditions in our seismometer gives an estimate for the r.m.s. value of the Brownian displacement of approximately 4.5 nm (45 Å). We do not have as yet typical figures for the noise originating in the photodetector, but we estimate on the basis of preliminary measurements that it is smaller than the Brownian noise. There is no way of reducing that part of the photodetector noise which lies within the signal passband. The Brownian noise, however, can be reduced by reducing the damping of the viscous or resistive type acting on the seismic mass ($z_n \to 0$ as $\alpha \to 0$, see Eq. (8)). Removal of damping would make the instrument practically useless as a seismometer. In order to make the instrument perform its function properly, it is then necessary to introduce an equivalent of damping by non-dissipative means, i.e., through the use of a feedback circuit which controls the position of the mass.

3. Feedback Control.

We adopted the feedback control as an essential part of the seismometer originally for the purpose of reducing the Brownian noise as explained above. On closer examination one finds that the feedback control offers several other advantages. First, the frequency response characteristic of the instrument with feedback becomes insensitive to changes in the period of the diamagnetic suspension. Second, the frequency passband of the feedback instrument can be varied over a large range by varying the parameters of the feedback loop. Indeed, the response can be made flat over a selected frequency range. Finally, the linearity may be improved and the dynamic range of the instrument extended.

The amount of electronic noise added by the feedback loop circuits is insignificant. The noise originating in the input circuit (including the electrooptical displacement sensor and its preamplifier) becomes amplified along with the signal. However, it can be shown that the signal-to-noise ratio remains unchanged. This is shown in a detailed analysis of the feedback seismometer in Appendix A. The principle of operation of the feedback-controlled seismometer may be described as follows.

Consider a seismic mass m suspended so that it is subject to a restoring force $K\zeta$ (K is the magnetic spring constant), velocity proportional damping force $\alpha\dot{\zeta}$ and an external (input signal) force f(t), (Figure 3).

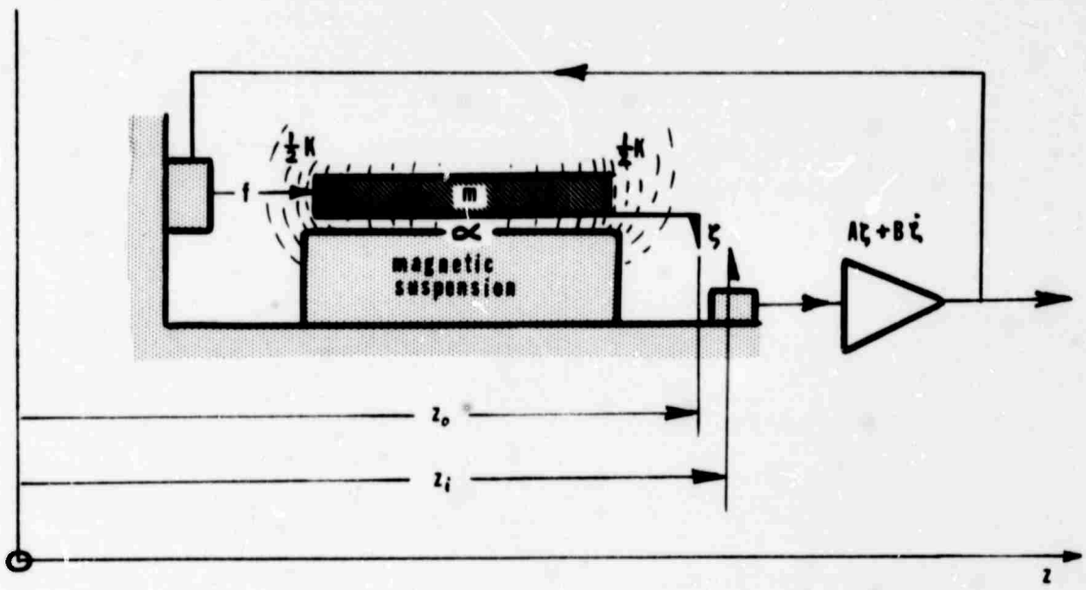

Fig. 3. Schematic diagram of the horizontal seismometer with feedback.

$\zeta = z_i - z_o$ is the displacement of the mass relative to the frame of the instrument, z_o is the coordinate of the mass in absolute (inertial) space, z_i is the coordinate of the frame in the absolute space.

With a feedback force $-f = A\xi + B\dot{\zeta}$, the equation of motion is

$$m\ddot{\zeta} + (\alpha + B)\dot{\zeta} + (K + A)\zeta = f(t). \qquad (9)$$

The effect of feedback is to change the spring constant and the damping. With feedback the seismometer will have a pendulous frequency $\omega_1 = \sqrt{(K+A)/m}$ and damping $\alpha+B$. If A and B are independently variable, the frequency response and damping can be adjusted at will. For instance, the so-called maximally flat or Butterworth frequency response is obtained when $(\alpha+A)^2 = 2\ m\ (K+B)$ or, if A and B are large compared to α and K respectively, $A^2 = 2mB$. The performance of the feedback instrument is then essentially independent of the parameters α and K of the original seismometer.

The design of the feedback loop is most readily done in the frequency domain. The basic components of the system and their transfer functions are shown in Figure 4.

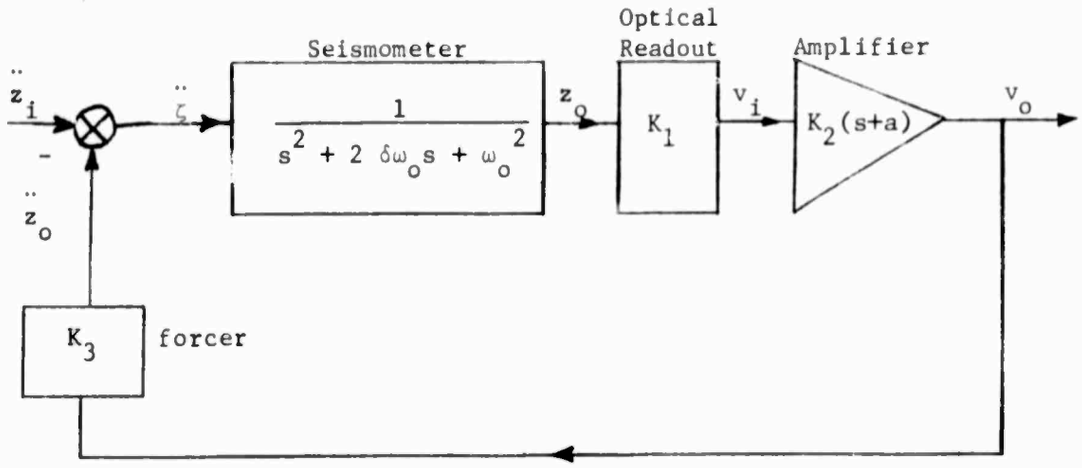

Fig. 4. Block diagram of the feedback loop circuit.

Here $\frac{1}{s^2 + 2\delta\omega_o s + \omega_o^2}$ is the acceleration-to-displacement transfer function of the seismometer, K_1 is the displacement-to-voltage constant of the optical readout, $K_2(s+a)$ is the voltage gain of the amplifier over the frequency range of interest, and K_3 is the voltage-to-acceleration constant of the feedback element or forcer. The overall closed loop transfer function is

$$\frac{v_o}{\ddot{z}_i} = \frac{K_1 K_2 (s+a)}{s^2 + (2\delta\omega_o + K_1 K_2 K_3)s + \omega_o^2 + K_1 K_2 K_3 a} \qquad (10)$$

When K_2 and a are adjusted to appropriate values, the frequency response of the closed loop system is as shown in Figure 5. It is flat to a frequency $\omega = a$ and the low frequency gain is $\frac{1}{K_3} + \frac{\omega_o^2}{K_1 K_2 a}$, or

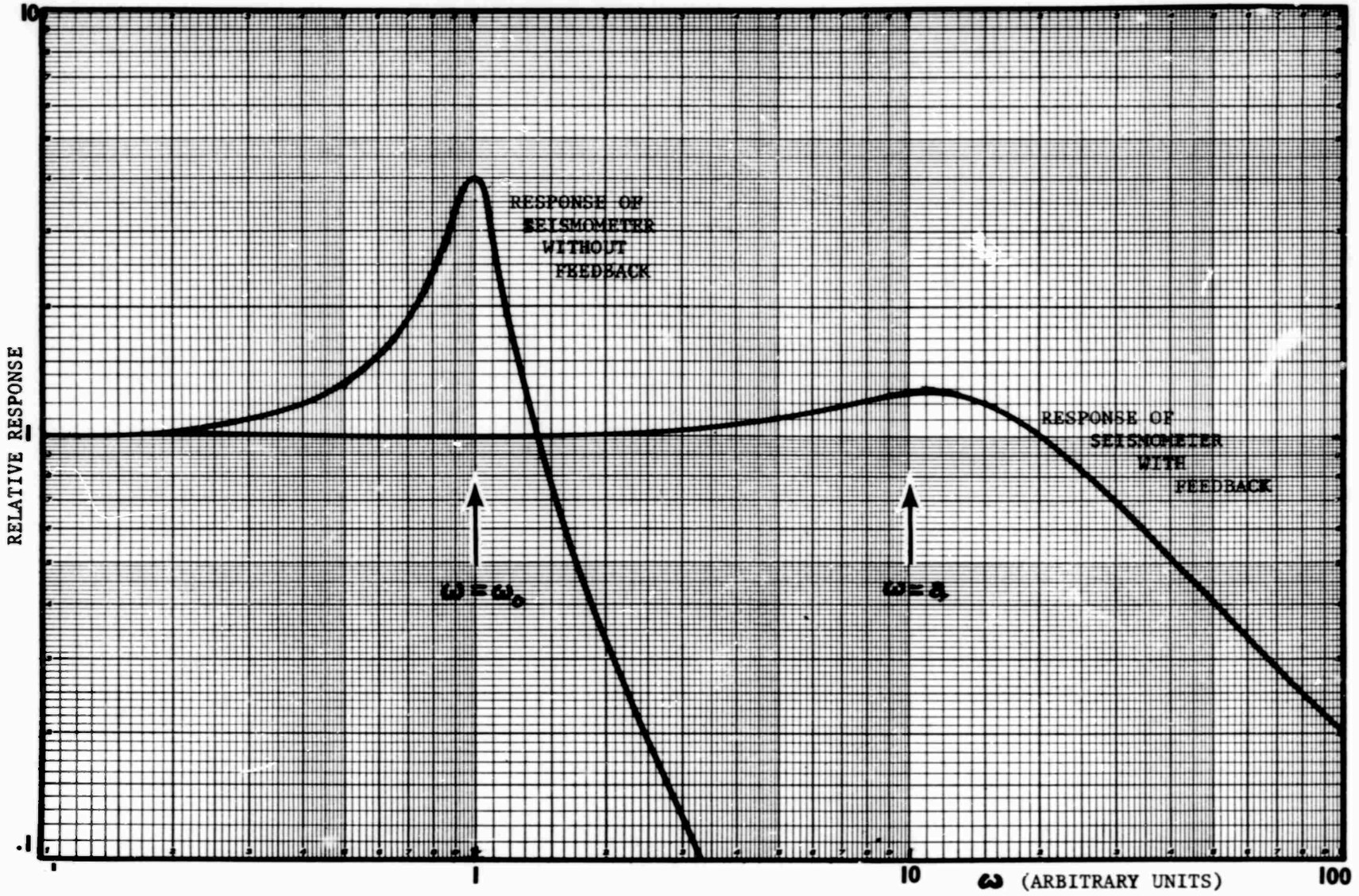

FIGURE 5 EFFECT OF FEEDBACK ON THE FREQUENCY RESPONSE OF SEISMOMETER

approximately $\frac{1}{K_3}$. The relative frequency response of the seismometer is also shown in Figure 5 for comparison. The low frequency gain in this case is $\frac{1}{\omega_o^2}$.

In this respect overall feedback serves to improve the linearity of the system since the linearity of the forcer can be considerably better than that of the seismometer and optical readout.

An amplifier transfer function of the form K(s+a) is not realistic since the gain cannot increase with frequency without limit. Therefore, in practice, the amplifier transfer function will be of the form K(s+a)/(s+b). Analysis of a feedback with this transfer function is somewhat more complicated than the previous case, but the important result one obtains is that damping of 70% or better can be obtained over a range of gain which increases with the frequency ratio b/a. This result is shown in Figure 6.

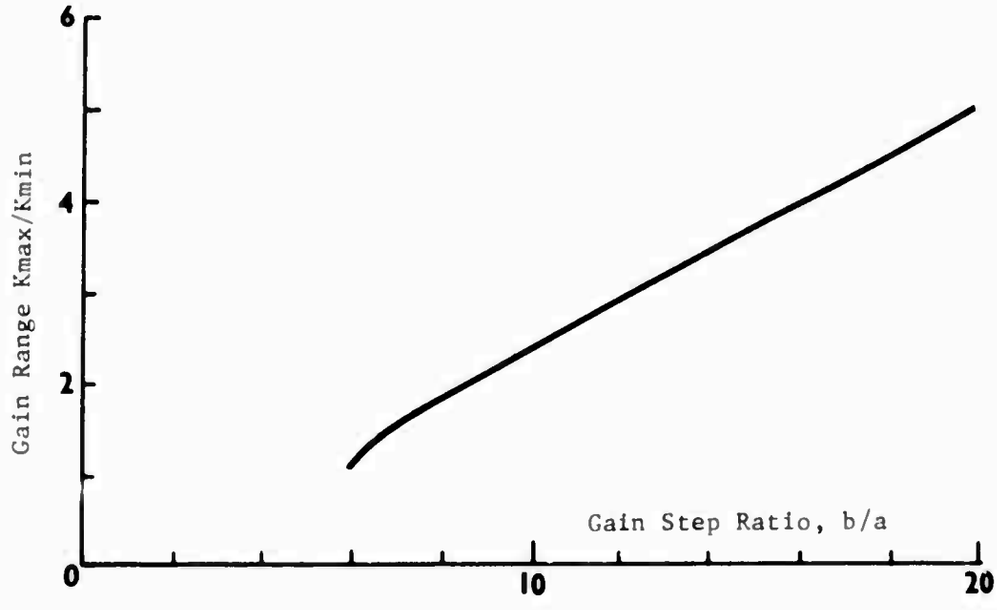

Fig. 6. Gain range required to obtain damping greater than 70% as function of gain step ratio.

B. INSTRUMENT CONSTRUCTION

The critical component of the magnetic suspension for the long-period horizontal seismometer is the set of polepieces that determine the field according to principles outlined in Section III,A1. The easier part of the problem is the cross-sectional geometry of the polepieces as outlined in Figure 2. This was worked out earlier and optimized by means of an analog field plotter so that a maximum supporting force was obtained for diamagnetic cylinders of the selected diameter (0.086 in.) with practically available permanent magnets. Shaping of the field along the sensitive axis is far more difficult since for long-period instruments the required field variation from center to end is typically one part in ten thousand or less. The initial approach was to give the gap a slight curvature along the axis by machining the edge of the lower polepiece. As it proved difficult to increase the period in this way beyond approximately six seconds, we decided to make the polepieces perfectly straight and as long as compatible with the overall size of the instrument. By making use of the lengthwise flux distribution in the polepieces and by adjusting the length of the graphite rod, we found it possible to make stable suspensions with a natural period of the seismic mass from 16 to 30 seconds.

The homogeneity of the polepiece material for long-period seismographs turned out to be rather critical for reasons of imperfections present in common stock of soft magnetic steels. Cold rolled Armco iron carefully inspected for flaws and voids was found adequate. The polepieces are fabricated from a round stock in one operation

without re-chucking while held between a dividing head and a center throughout the entire machining operation. The polepiece-and-magnet assembly was shown in Figure 2 of our Second Quarterly Report dated 31 December 1967.

Overall view of the complete horizontal seismometer is shown in Figure 7. The upper part is the seismometer proper(S), the middle part is the remote levelling jack screw (RL), and the bottom part is the piezoelectric forcer or tilt platform (PZT). The instrument is housed inside a 4.25 in. I.D./4.75 in. O.D. iron casing (C) with gas-tight lids and cable feedthrough. Besides its protective function the casing serves as a magnetic shield. Assuming permeability μ = 1000 its shielding factor should be better than 50.

The "C" shaped Alnico V magnets used in the seismometer are 2.50 in. wide and are shaped to fit the angular polepieces of 3.25 in. axial length. The "C" magnets adhere strongly to the polepiece structure by magnetic attraction and the assembly is fastened to the base by means of clamps and set screws on the magnets.

The graphite rods are machined from 0.125 in. diameter spectroscopic grade graphite to a diameter of 0.086 in. with a diamond tool. The rods must be thoroughly cleaned by boiling in 1:1 hydrochloric acid, ultrasonic cleaning in detergent, and boiling in several changes of distilled water. The graphite easily picks up enough iron contamination from the machining operation to make it behave erratically in the magnetic field.

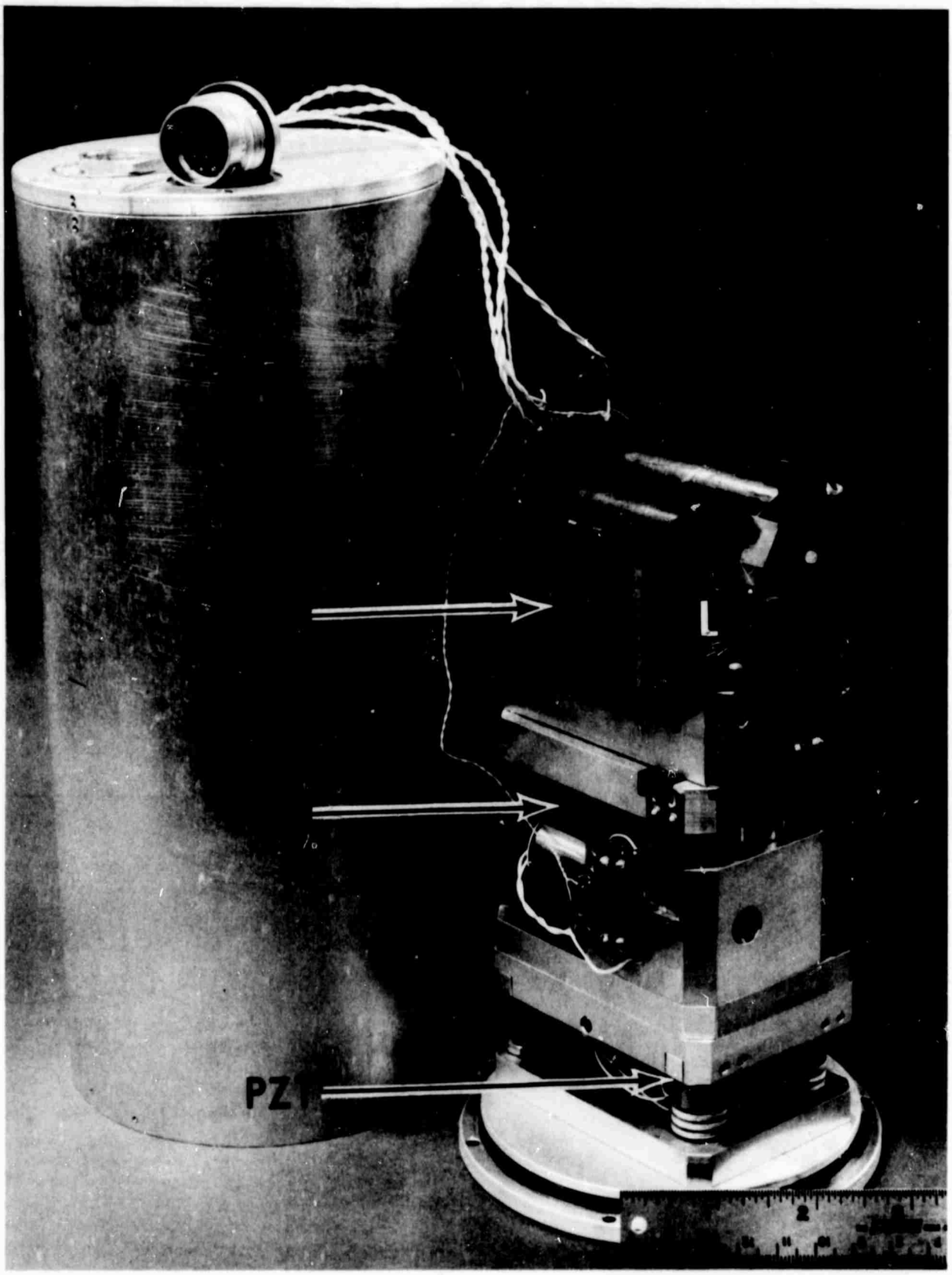

FIGURE 7 VIEW OF THE COMPLETE HORIZONTAL SEISMOMETER

The optical readout (Figure 8) consists of a light source (L), a light obstructing "flag" (F) attached to the graphite rod and dual photodetector (PD) of the cadmium sulfide (CdS) photoresistive type. The lamp is a selected T-1 size, 5 volt bulb rated for a 10^5 hours' life service. The CdS photodetector is a standard CL 705 L/2 Clairex cell. The lamp and cell are provided with glass light pipes. The light, after passing past the flag, is conducted to the two halves of the photoconductive cell by curved (90°) rectangular light pipes (LP). This arrangement permits us to place the photocell proper inside one of the magnets to save space.

Levelling of the instrument after it is placed in a borehole is provided by a motor-operated jack screw assembly located immediately below the seismometer assembly. The motor leveller has a range of approximately ±2° and operates on a one- to five-volt D.C. bipolar source. The motor is a PM-field D.C. motor with a 560:1 gear reduction. There is a 20:1 worm gear reduction following this which turns a 40-pitch precision ground jack screw. With five volts applied, the jack screw moves about .001 inches per minute. This corresponds to a tilt of 400 microradians per minute. We find that the motor leveller is sensitive enough in its operation to be used as an intermediate levelling device such as a drift corrector to keep the trace on the chart paper. This is presently accomplished by using high and low limit switches on the recorder which activate the motor.

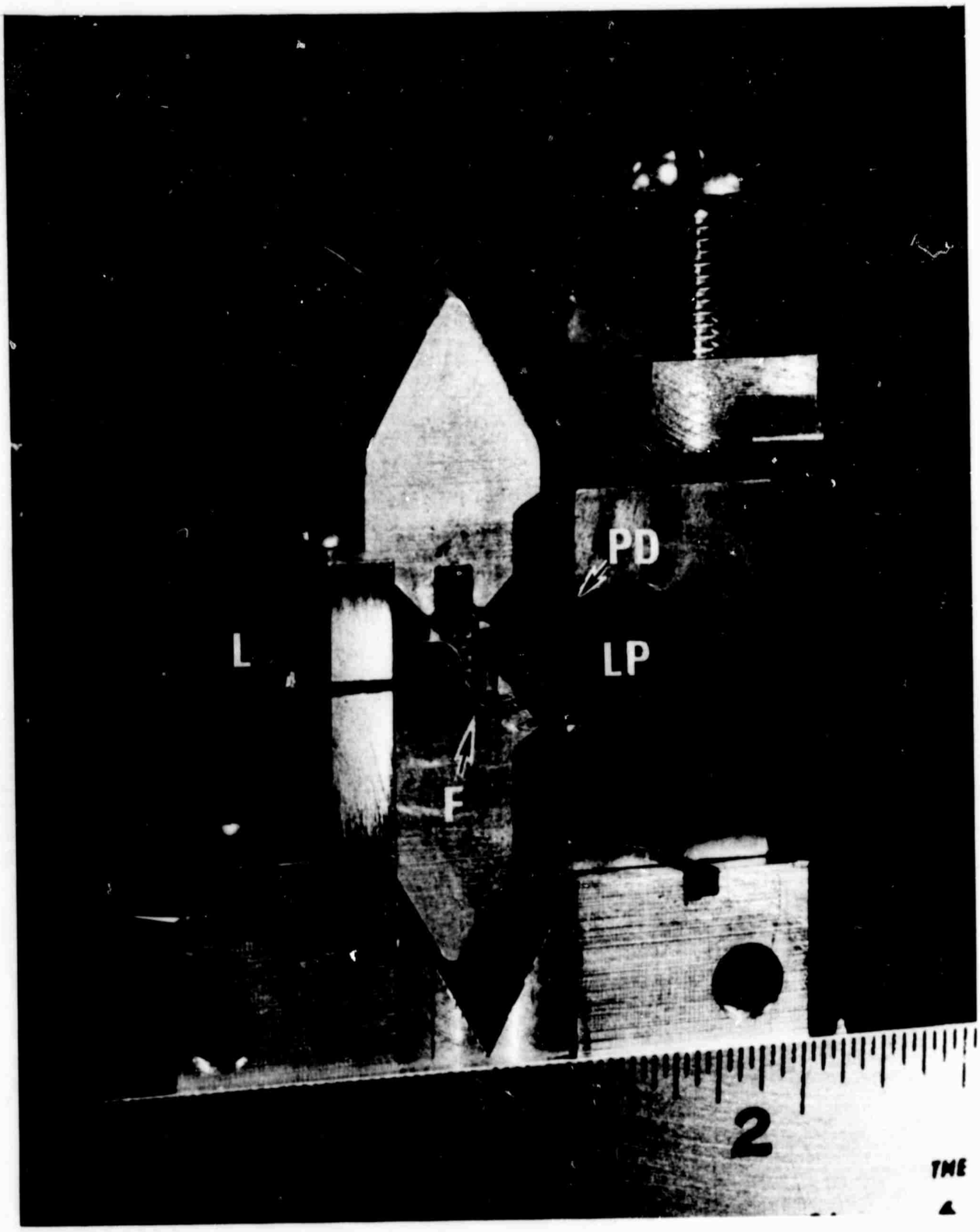

FIGURE 8 VIEW OF THE OPTICAL READOUT OF THE HORIZONTAL SEISMOMETER

The piezoelectric tilt table located under the motor-operated leveller is used in the feedback loop to deliver the controlled force acting against the inertial force from the input acceleration. If the table is tilted by an angle θ, the force acting on the seismic mass is mg sin θ, or approximately mg θ. The tilting is obtained by three stacks of piezoelectric ceramic discs arranged so that application of a ±100 volt control voltage tilts the seismometer by ±5 microradians. In terms of the feedback circuit, Figure 4, this corresponds to a forcer constant $K_3 \simeq 5 \times 10^{-5}$ cm sec^{-2} volt^{-1}.

A typical horizontal seismometer has a natural frequency, $\omega_o \simeq 0.4$ rad/sec (16-second period) and is lightly damped ($\delta \simeq 1/8$), so that its transfer function is

$$\frac{z_o}{\ddot{z}_i} = \frac{1}{s^2 + .08s + .16} \quad . \tag{11}$$

The optical readout constant, K_1, is about 20 volts/cm. The feedback amplifier was designed with both the gain and the frequency of the gain step adjustable over wide ranges. At present the gain step is fixed at 10 (20db) to allow for a 2:1 gain variation with acceptable damping. The operating settings result in a voltage transfer function for the amplifier approximately

$$\frac{v_o}{z_i} = 10^4 \frac{s + 2}{s + 20}$$

and the closed loop instrument is slightly underdamped.

The circuit diagram of the horizontal feedback circuit is shown in Figure 9.

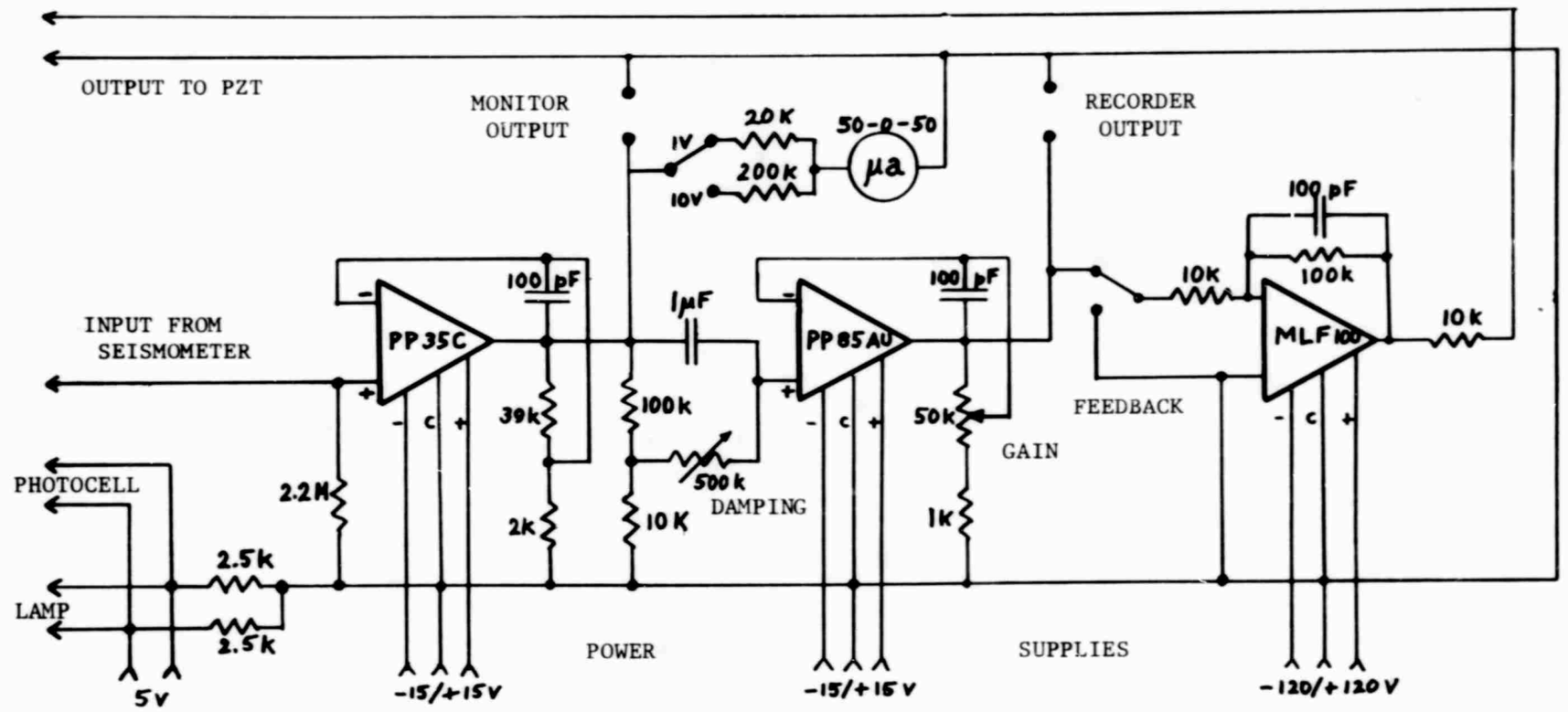

FIGURE 9 HORIZONTAL SEISMOMETER FEEDBACK CIRCUIT

IV. VERTICAL SEISMOMETER

A. OPERATING PRINCIPLE

The vertical seismometer makes use of a magnetic field suspension of a type quite different from that employed in the horizontal units. Analysis shows that the vertical suspension of the diamagnetic seismic mass having the required long period would require extremely close tolerances on the exact shape of the field and it would support still smaller masses than those used in the horizontal diamagnetic suspension.

The suspension chosen for the vertical seismometer is of a hybrid type consisting of magnetic dipole suspension for the seismic mass and a pair of diamagnetic guides, schematically outlined in Figure 10.

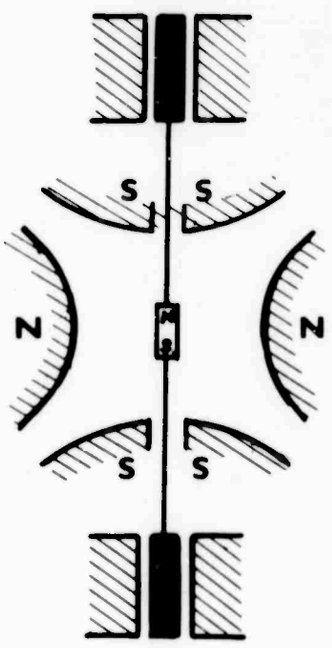

Fig. 10. Schematic diagram of the vertical magnetic suspension.

The seismic mass contains a permanent magnet of a dipole strength μ which is suspended in a magnetic field having a vertical gradient such that the upward force acting on the dipole is equal to the weight of the seismic mass:

$$\mu \frac{\partial H_z}{\partial z} = mg. \tag{12}$$

The suspension is unstable inasmuch as the dipole has the tendency to flip over at a slightest departure from exact symmetry. This is prevented by the two diamagnetic guides which act as noncontacting (frictionless) sleeve bearings. They consist of graphite cylinders supported by magnetic fields of a quadrupole configuration.

The entire structure is symmetric about a vertical axis and the seismic mass is constrained to move along this axis in the vertical direction.

The main field supporting the mass may be described by a magnetic potential Ω represented by a sum of cylindrical harmonics satisfying the Laplace's equation. If we consider only the first three harmonics, the magnetic potential Ω has the general form:

$$\Omega = Az + B(2z^2 - r^2) + C(2z^3 - 3r^2z) \tag{13}$$

where A, B, and C are adjustable constants.

The field components are:

$$H_z = -\frac{\delta\Omega}{\delta z} = -A - 4Bz - C(6z^2 - 3r^2) \tag{14}$$

$$H_r = -\frac{\delta\Omega}{\delta r} = 2Br + 6Crz \tag{15}$$

The potential energy of the dipole in the field H is

$$-(\vec{\mu} \cdot \vec{H}) = \mu \left(H_z \cos\theta + H_r \sin\theta \cos\phi\right) \qquad (16)$$

where θ is the inclination of the dipole axis to the z-axis and ϕ is the azimuth of the inclined dipole. In (16) the north pole of the dipole is assumed to be directed downwards.

The potential energy of the two graphite cylinders is

$$V' = \chi' v' H'^2 \qquad (17)$$

where χ' is the diamagnetic susceptibility of graphite, v' is the total volume of the two cylinders, and H' is the quadrupole field in each bearing. The magnetic potential for these quadrupole fields is $\Omega \propto r^2 \cos 2\phi$ and the field components are $H_r \propto r \cos 2\phi$, $H_\phi \propto r \sin 2\phi$.

Thus

$$H' = H'_m \, r'/a \qquad (18)$$

where H'_m is the magnetic field at the quadrupole pole-faces of radius a.

The displacements of the upper and lower diamagnetic cylinders due to the tilt of the suspended assembly are given by

$$r_2'^2 = r^2 + 2\ell r \sin\theta \cos\phi + \ell^2 \sin^2\theta \qquad (19)$$

$$r_1'^2 = r^2 - 2\ell r \sin\theta \cos\phi + \ell^2 \sin^2\theta \qquad (20)$$

where r'_2, r'_1 are the radial positions of the centers of the two cylinders, r is the position of the permanent dipole, and 2ℓ is the distance

between the centers of the cylinders. The potential energy of the two cylinders is therefore, from (17) and (18),

$$V' = \frac{\chi' v' H_m'^2}{a^2} (r_2'^2 + r_1'^2)$$

$$= \frac{2\chi' v' H_m'^2}{a^2} (r^2 + \ell^2 \sin^2\theta) \qquad (21)$$

Thus, the total magnetic potential energy of the suspended system is

$$V = \frac{2\chi' v' H_m'^2}{a^2} (r^2 + \ell^2 \sin^2\theta) + \mu(H_z \cos\theta + H_r \sin\theta \cos\phi) \qquad (22)$$

When the supporting field is defined by the potential of Eq. (13), the components H_z and H_r are given by (14) and (15). Therefore, V becomes

$$V = \frac{2\chi' v' H_m'^2}{a^2} (r^2 + \ell^2 \sin^2\theta)$$

$$+ \mu\cos\theta \left[- A - 4Bz - C(6z^2 - 3r^2)\right]$$

$$+ \mu\sin\theta \cos\phi \left[2Br + 6Crz\right] \qquad (23)$$

We can determine the constants A, B, and C by considering the case $r = 0$, $\theta = 0$. Then

$$V = - \mu A - 4\mu Bz - 6\mu Cz^2 \qquad (24)$$

On applying the conditions at z = 0, that

$$H = H_0 \tag{25}$$

$$-\frac{\partial V}{\partial z} = W \tag{26}$$

$$\frac{\partial^2 V}{\partial z^2} = K \tag{27}$$

we obtain

$$A = -H_0 \, , \; B = \frac{W}{4\mu} \, , \; C = -\frac{K}{12\mu} \tag{28}$$

The potential energy of the suspended sy tem can therefore be written as:

$$V = \frac{2\chi' v' H_m'^2}{a^2} (r^2 + \ell^2 \sin^2\theta)$$

$$+ \cos\theta \left[\mu H_0 - Wz + \frac{K}{12} (6z^2 - 3r^2) \right]$$

$$+ \sin\theta \cos\phi \left(\frac{W}{2} r - \frac{K}{2} rz\right) \tag{29}$$

For small values of the variables z, r, θ, and ϕ we find

$$V = \mu H_0 + \frac{1}{2} Kz^2 + \left(\frac{2\chi' v' H_m'^2}{a^2} - \frac{K}{4} \right) r^2 + \frac{1}{2} Wr\theta$$

$$+ \left(\frac{2\chi' v' \ell^2 H'^2}{a^2} - \frac{\mu H_0}{2} \right) \theta^2 \tag{30}$$

Note that ϕ enters only in terms higher than second order.

Stability requires that V must increase from its equilibrium value of μH_0 for any arbitrary combination of z, r, and θ. The necessary conditions are

$$\frac{2\chi' v' H_m'^2}{a^2} > \frac{K}{4} \tag{31}$$

$$\frac{2\chi' v' \ell^2 H_m'^2}{a^2} > \frac{\mu H_0}{2} \tag{32}$$

$$\left(\frac{2\chi' v' H_m'^2}{a^2} - \frac{K}{4}\right)\left(\frac{2\chi' v' H_m'^2}{a^2} - \frac{H_0}{2}\right) > \frac{1}{16} W^2 \tag{33}$$

Condition (31) has to do with pure radial displacement, (32) with pure rotation, and (33) with combined rotation and radial displacement.

It is to be noted from (30) that although there is coupling between r and θ, there is no interaction of these coordinates with z. This fortunate state of affairs is only realizable with the field defined by (13). Any field more complicated than this will produce cross-coupling. On substituting from (28) into (14) we find for the required field on the axis:

$$H_z = H_0 - \frac{W}{\mu} z + \frac{K}{2\mu} z^2 \tag{34}$$

A field of this type has equipotential surfaces of the form of a hyperboloid of revolution with asymptotes defined by

$$z = \pm \frac{1}{\sqrt{2}} r. \tag{35}$$

This is tne field we actually use in the vertical seismometer.

A field of this geometry can be realized with a set of polepieces having equipotential contours according to Eq. (34). The polepiece set having a shape of a hyperboloid of revolution is energized by permanent magnet rings placed at appropriate locations around the working gap.

Even though this type of suspension can suspend considerably larger seismic masses than the diamagnetic suspension, we followed the same general philosophy in the overall design of the vertical seismometer. In particular, we decided to provide the instrument with feedback control for the same reasons as with the horizontal instrument. Detailed analysis of the vertical feedback seismometer is given in Appendix A.

B. INSTRUMENT CONSTRUCTION

The vertical magnetic suspension system forms a self-enclosed unit contained in a heavy-walled soft iron tube 3.5 inches in diameter which serves both as a return flux path and a structural frame of the instrument. To it are bolted the two quadrupole magnet systems that guide the suspended dipole along the vertical axis and prevent its tipping over due to the inherent instability. The complete seismometer is shown in Figure 11 and some of its essential parts are shown disassembled in Figure 12. The seismometer fits in a standard 4.75 in. O.D. steel

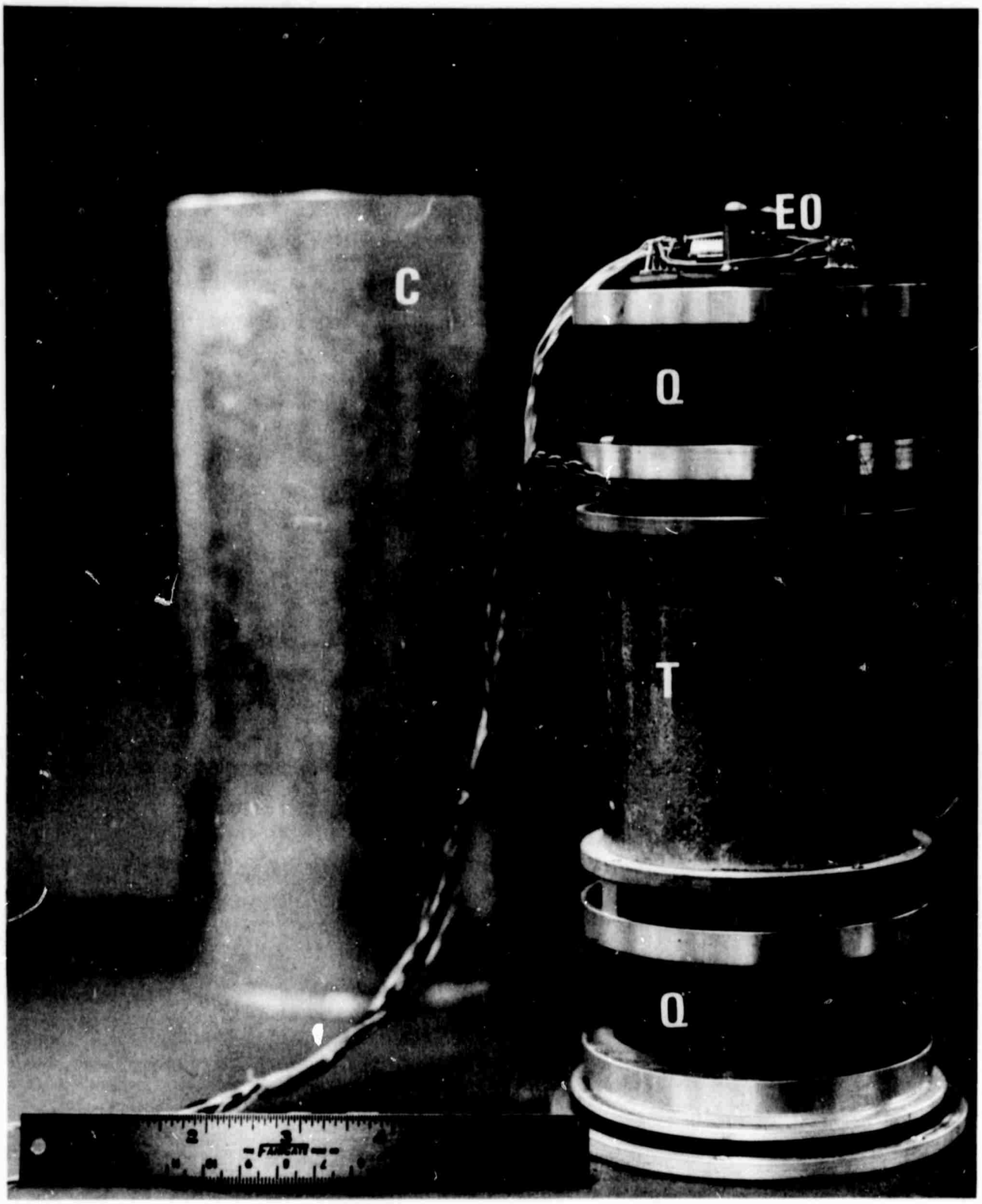

FIGURE 11 VIEW OF THE COMPLETE VERTICAL SEISMOMETER

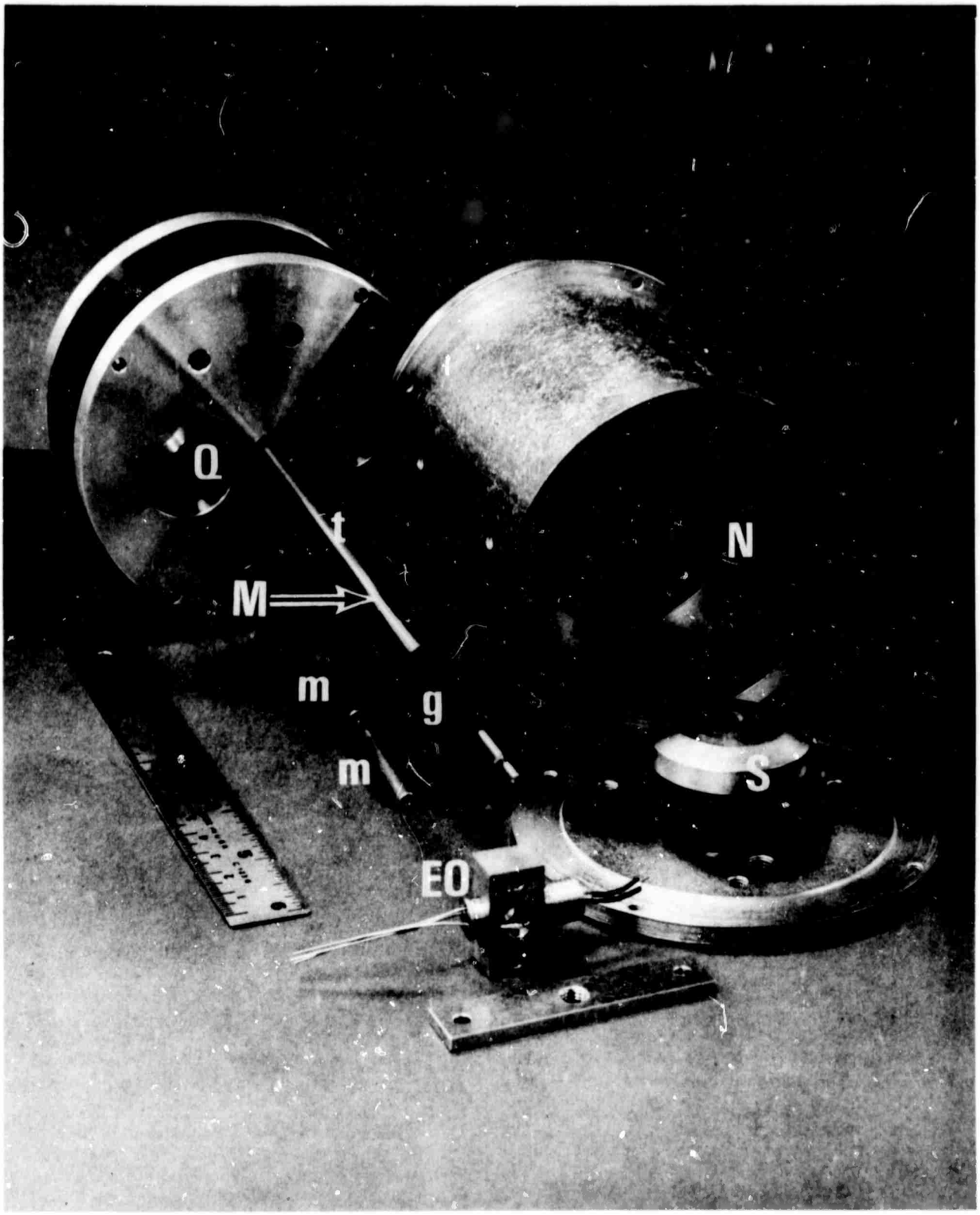

FIGURE 12 VIEW OF THE COMPONENTS OF THE VERTICAL MAGNETIC SUSPENSION

case (C) which serves again as a magnetic shield. The construction is simplified somewhat by the fact that the instrument need not be levelled to the narrow limit required by the horizontal seismometer. The present model tolerates deviations from the vertical of approximately ±1 degree and we are trying to extend this to ±2 degrees by strengthening the quadrupole systems Q. Consequently, we do not plan to use any remote levelling system for the vertical seismometer.

The electrooptical readout system (EO) is mounted on the top of the instrument. It consists of a light source and a dual photocell of the same type as in the horizontal instrument. The vertical motion of a disc-shaped light obstruction attached to the upper end of the seismic mass controls the distribution of light between the two halves of the CdS photodetector.

Referring to Figure 12 we see the suspension magnet system (partially opened) showing the upper polepiece (S) attached to a ring-shaped Alnico V permanent magnet. The circular polepiece (N) represents only a fraction of the theoretical hyperboloid contour; however, this is found to be satisfactory in practice. The upper and lower polepieces (S) are provided with 0.25 in. diameter axial holes to permit the passage of the seismic mass assembly (M) through them. The seismic mass consists of several parts held together by a length of a 0.187 in. O.D., 0.005 in. wall stainless steel tubing (t). In the center of the tube is fixed the suspended dipole which has a form of cylinder 0.177 in. O.D., 0.375 in. long made of sintered Alnico VIII; this material has

sufficiently high coercive force ($\sim$1600 Oe) to minimize the undesirable effect of position-dependent induced magnetization.

The upper and lower ends of the stainless steel tube hold two graphite rods (g), 0.187 in. O.D., which serve as diamagnetic guides for the suspended seismic mass. The mass is augmented by two brass slugs (m) which fit closely in the tube and the weight of which is adjusted roughly so that Equation (12) is fulfilled. Fine adjustment of the gradient is done by means of magnetic shunt screws adjacent to the Alnico V ring magnets (not shown in the picture). Fine adjustment of the second-order term (Eq. 19) which determines the spring constant of the suspension is made by means of a thin coil located in the plane of the ring (N); by adjusting the current through this coil the period can be set to any desired value. At present the period is set to approximately 2.5 seconds. Another coil ("motor" coil) serves to produce a small variable gradient for the purpose of applying a control force on the suspended dipole. The complete set of coils (not shown in Fig. 11) fits coaxially with the seismic mass assembly in the working space of the suspension magnet assembly.

The feedback system for the vertical seismometer is similar to that for the horizontal instrument in principle but differs in several details. The circuit diagram is shown in Fig. 13. To allow for a possible 4:1 change of gain with period, a gain step of 16 (24 db) was used. The gain and the frequency of the gain step are adjustable. The output current is fed back to the motor coil of the seismometer. The feedback loop includes an integrating amplifier which provides high gain at very low frequencies,

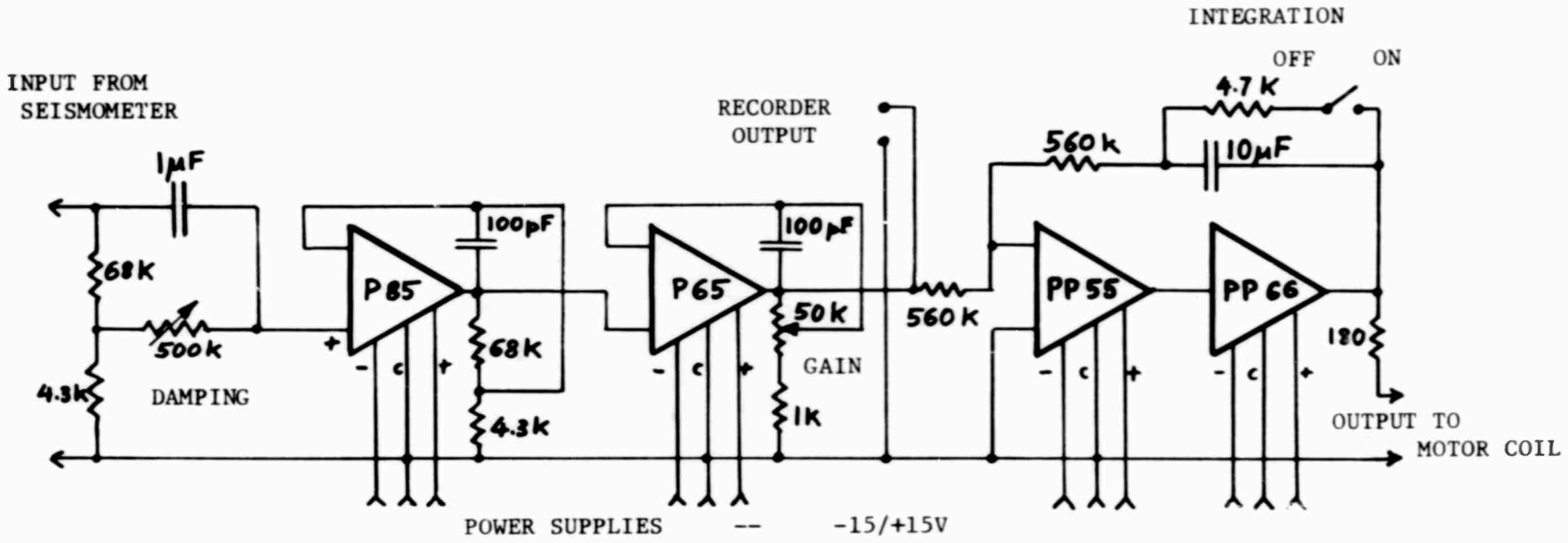

FIGURE 13 VERTICAL SEISMOMETER FEEDBACK CIRCUIT

below the band of interest. The effect of this integration is to lower the overall response at these low frequencies and thus minimize the drift of the center point of suspension.

V. BOREHOLE INSTRUMENT PACKAGE

For borehole installation the two horizontal seismometers and the vertical seismometer are combined in one unit schematically outlined in Figure 14. This package is still under construction and has not been tested as yet. It consists of a stainless steel tube 5.50 in. O.D., .120 in. wall. approximately 40 in. long with a welded bottom and an O-ring sealed header with watertight cable feedthroughs. The three instruments are stacked in this tube and bolted together with .2 in. spacer rings. The upper ring has an expandable section to assure firm coupling to the wall of the tube which in turn is eventually coupled to the casing of the borehole. We are presently planning to use Ser. SW borehole casing of 6 in. I.D. and 6-5/8 in. O.D. for down-hole testing of the instrument. The upper part of the instrument package is coupled to the borehole casing by a suitable hole lock. We have not yet made the final decision whether to use a simple tension release-operated lock or a motor-driven one. Three multi-conductor cables will connect the instrument with a junction box and the electronics console on the surface. Even though we expect to have a "dry"-cased borehole for the tests, the instrument package and the cabling will be constructed to be watertight.

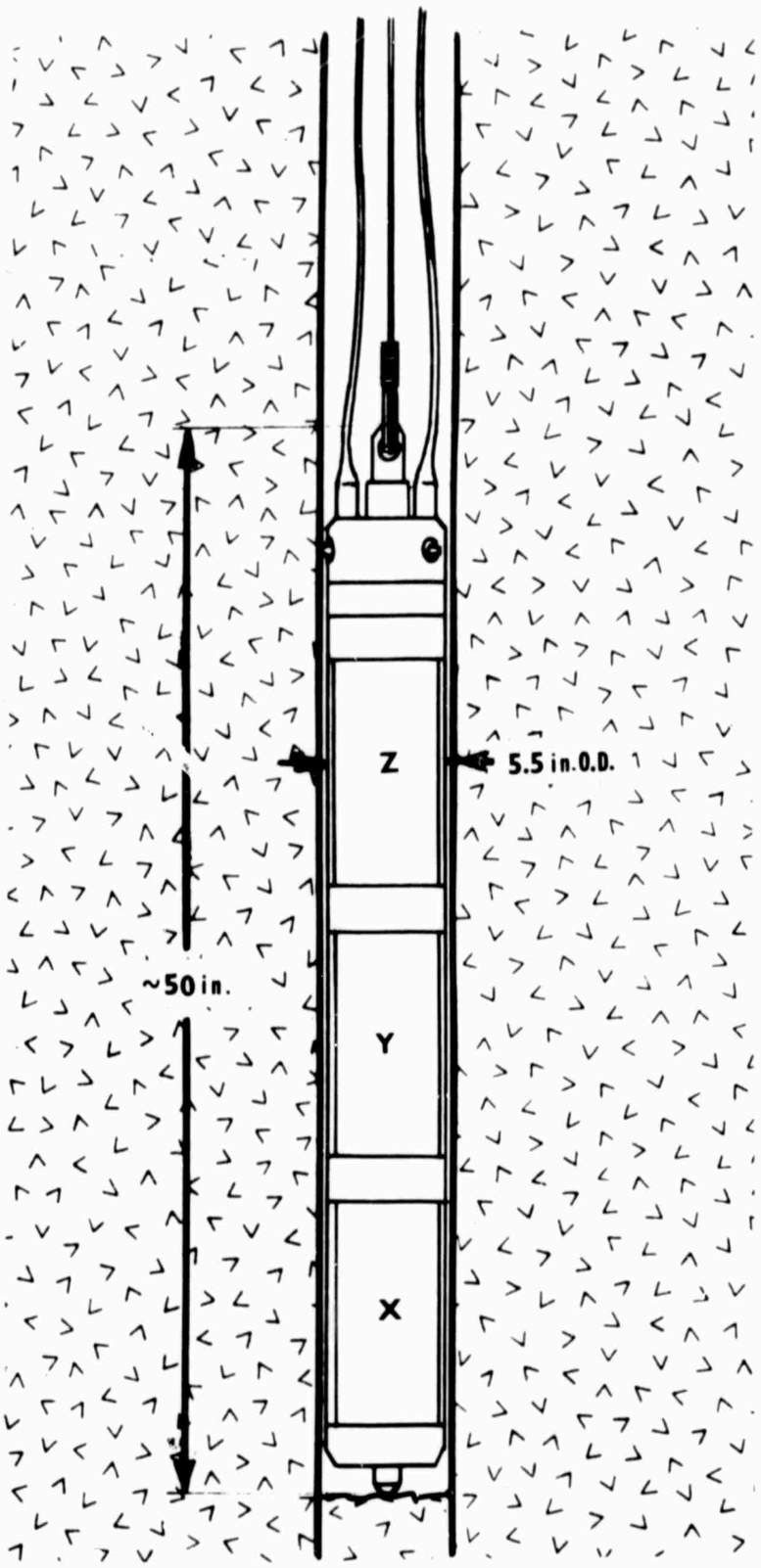

FIGURE 14 OUTLINE OF THE THREE-COMPONENT BOREHOLE SEISMOMETER

VI. PRELIMINARY TEST RESULTS

A. FREQUENCY RESPONSE OF THE SEISMOMETERS

Tests reported below are of a preliminary nature inasmuch as they have been performed on first-of-a-kind experimental instruments and their purpose was mainly to ascertain whether or not the instruments perform according to the design goals. Also, the parameters of filter networks that will be eventually used for shaping of the passband have not been finalized at the time of the tests. For this reason the frequency response of the horizontal seismometer was tested without any filters outside the feedback electronics.

The horizontal instruments were tested on a rocking platform producing an acceleration of a constant amplitude (approximately 6.4×10^{-6} g) and variable frequency (from .008 to 1 Hz). Alternately, we applied a low frequency test voltage on the PZT crystals actuating the tilt platform. High amplitude of the test signal was necessary in order to maintain a sufficiently high signal-to-noise ratio at the high ground noise level prevailing at the Acorn Park laboratories.

A typical test result is shown in Figure 15. Both amplitude and phase response are plotted on the diagram. The instrument was a horizontal seismometer No. C-2 operated with the feedback circuit described earlier (Section III).

Results of a similar test made with a vertical seismometer No. VS-2 are shown in Figure 16. Since we did not have a shake table

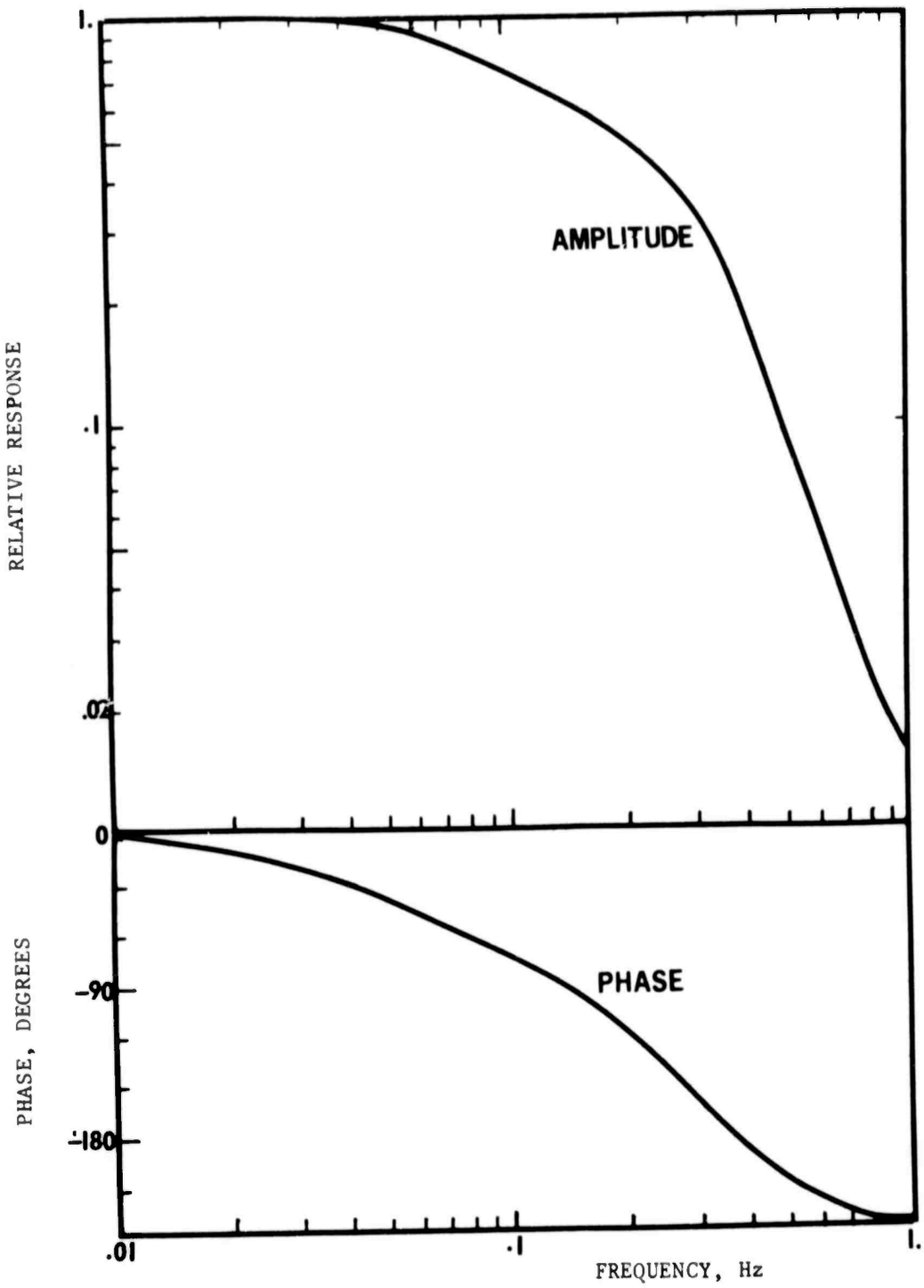

FIGURE 15 FREQUENCY RESPONSE OF THE HORIZONTAL SEISMOMETER C-2 WITH FEEDBACK, TESTED AT CONSTANT ACCELERATION

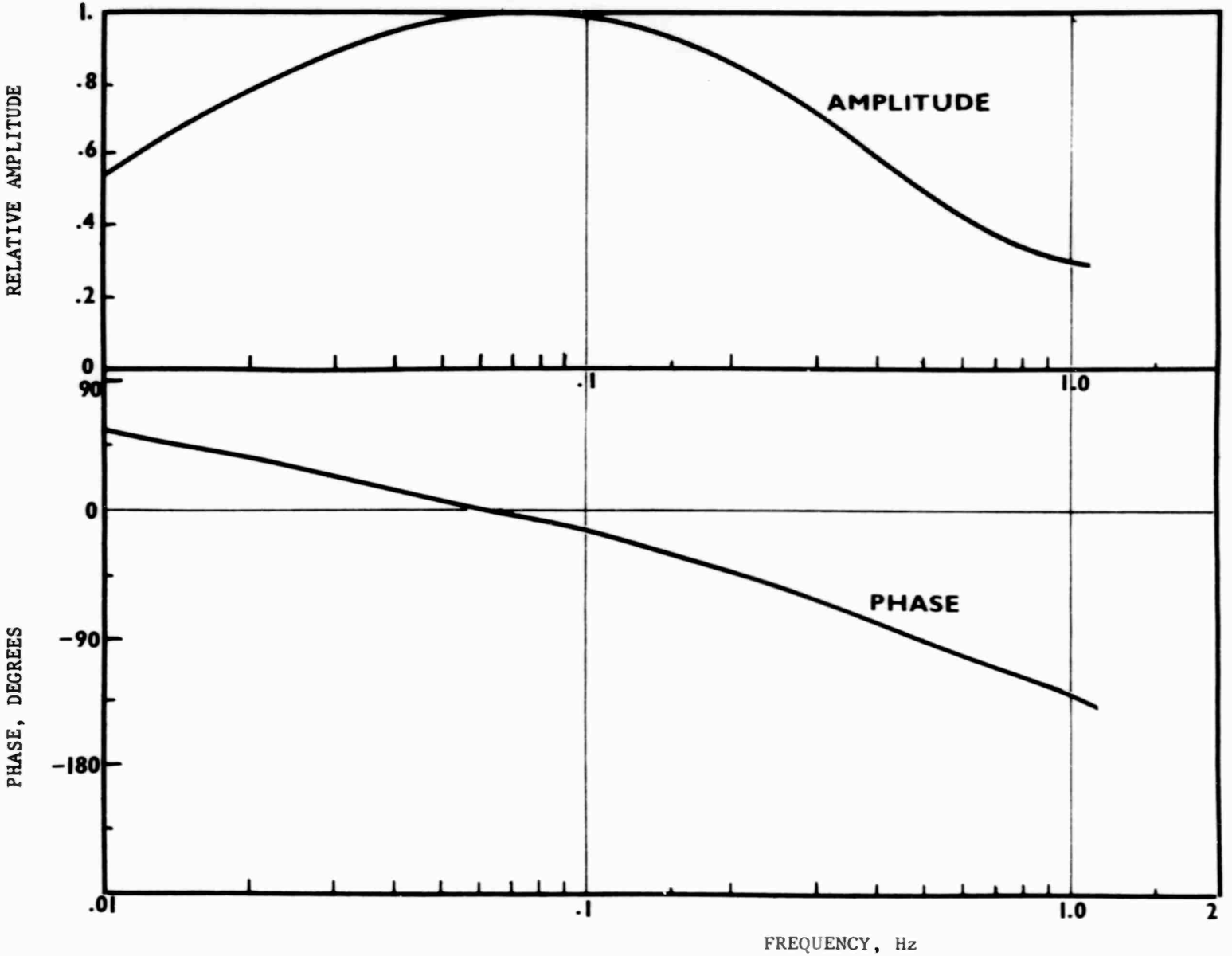

FIGURE 16 FREQUENCY RESPONSE OF THE VERTICAL SEISMOMETER VS-2 WITH FEEDBACK, TESTED AT CONSTANT ACCELERATION

operable over the required low frequency range, we used an indirect method. A test signal derived from a low frequency function generator (Hewlett-Packard Mod. 202A) was fed into one of the motor coils to generate a frequency-variable force of essentially constant amplitude acting on the seismic mass. Consequently, tests performed in this way yield frequency response versus acceleration characteristics. The curves plotted in Figure 16 were obtained with the vertical seismometer operated with a feedback circuit according to Figure 13. A simple low pass filter with a cutoff frequency of approximately 1 Hz was used in this test at the signal output.

B. SAMPLE SEISMOGRAMS

During the laboratory tests at Acorn Park (Cambridge, Massachusetts) teleseismic events were occasionally recorded. Because of the seismologically unfavorable characteristics of the site (swampy ground without connection to bedrock, combined with a very high level of natural and man-made ground noise) the instruments could never be operated at high gain. Consequently, only large events ($M > 6.5$) were recorded. Also, since no effort was made to operate the instruments continually, many events undoubtedly escaped our attention. Under these conditions obtaining a good record was a matter of chance. A sample of one of the best recordings obtained with the horizontal feedback seismograph is shown in Figure 17. The event was an earthquake ($M \approx 7$) off Hokkaido, Japan, which occurred at 10:39:01.6 on 16 May 1968. The epicenter was identified from the C.G.S. - P.D.E. cards. The record is good enough to permit clear identification of most of the typical phases present.

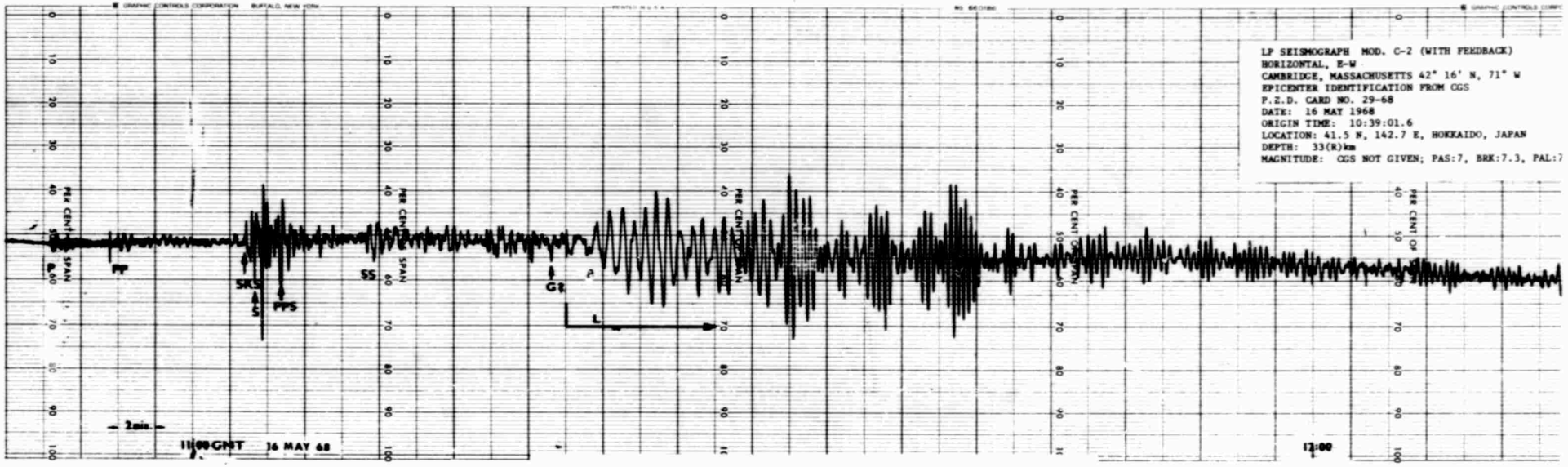

FIGURE 17 PART OF THE RECORDING OF A TELESEISMIC EVENT MADE WITH THE C–2 HORIZONTAL FEEDBACK SEISMOGRAPH

APPENDIX A

ANALYSIS OF FEEDBACK VERTICAL SEISMOMETER

In the development of the vertical seismometer using magnetic suspension and feedback, calculations on the response of the system to the following input signals have been made: vertical displacement of the frame; tilting of the frame; Brownian motion of the seismic mass, and electronic noise.

APPENDIX A

TABLE OF CONTENTS

I. INTRODUCTION AND SUMMARY

The attached series of calculations is an attempt to collect in one document the analysis that has been done over the last year on the development of a fedback magnetically supported vertical seismometer. It should be emphasized that this is a preliminary and incomplete attempt. The present work still requires editing to be concise and internally consistent. In addition, the work requires extension so that hard and fast design decisions can be made.

Two tentative designs are sketched; one employing positive feedback to increase the natural period of the instrument, and negative feedback to reduce drift. This design, described as design A in section XI, requires wide dynamic range in mass displacement, and its output is sensitive to detector sensitivity and amplifier gain variations.

The second design, suggested by Martin Cohen, is fed back negatively over the full range of operating frequencies. Its gain is a function only of the force constant of the instrument and is independent of detector sensitivity and amplifier gain.

II. FEDBACK VERTICAL SEISMOMETER

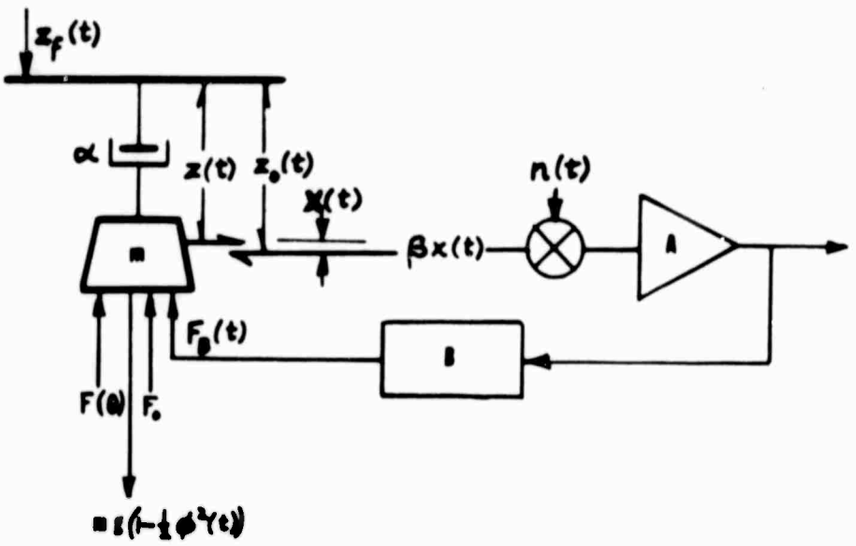

FIGURE II-1. DIAGRAM OF FEDBACK VERTICAL SEISMOMETER

where

$Z_f(t)$ = the time varying displacement of the frame (cm)

$Z(t)$ = the time varying displacement of the mass m with respect to the frame (cm)

Z_o = the equilibrium position of the mass m with respect to the frame (cm)

$X(t)$ = $Z(t) - Z_o$ (cm)

β = detector sensitivity (volts/cm mass displacement)

$\eta(t)$ = equivalent input electrical noise to the system volts

A = amplifier gain

$O(t)$ = output signal volts

B = feedback factor cm^{-1}/volt

F_B = feedback force (dynes)

F_o = static supporting force (dynes)

mg = static gravitational force (dynes)

$\frac{-mg\phi^2(t)}{2}$ = tilt force (dynes)

$\phi(t)$ = tilt angle relative to the vertical (radians)

$F(\theta)$ = Brownian force (dynes)

θ = temperature (degrees absolute)

Considering the total vertical acceleration of the seismic mass m to be the acceleration of the frame plus the acceleration of the mass relative to the frame, one can write a general force balance equation of the form

$$m\ddot{X} + \alpha\dot{X} = -m\ddot{Z}_f + F_o + F(\Theta) + F_B(t) - mg\left(1 - \frac{\phi^2(t)}{2}\right) \qquad \text{(II-1)}$$

III. MAGNETIC FIELD DESIGN AND ADJUSTMENT

If the magnetic field is configured so that

$$H(X) = H_o \left[\{a + b(t)\} X - \frac{c}{2} X^2 \right] \qquad \text{(III-1)}$$

and further, if the seismic mass m is given a magnetic dipole strength of μ, then the vertical magnetic force on the mass will be given by

$$F_o + F_B(t) = \frac{\mu \partial H(X)}{dX} = \mu H_o \left[a + b(t) - c \cdot X(t) \right] \qquad \text{(III-2)}$$

where

F_o = static supporting force (dynes)

$F_B(t)$ = time varying fedback force (dynes)

μ = magnetic dipole strength of seismic mass (dyne $\cdot$ cm $\cdot$ gauss^{-1})

H_o = magnetic field at equilibrium point, i.e., X=o (gauss)

a = static field strength adjustable parameter (cm^{-1})

b(t) = dynamic field strength adjustable parameter (cm^{-1})

c = static field curvature adjustable parameter (cm^{-2})

Referring to equation (II-1) and equating static terms, at X=o, one obtains

$$F_o = \mu H_o a = mg \qquad \text{(III-3)}$$

To adjust the operating point at X=o, one adjusts the static parameter a so that

$$a = \frac{mg}{\mu H_o} \qquad \text{(III-4)}$$

Assuming this adjustment, equation (II-1) can be rewritten in the form

$$\ddot{X} + \frac{\alpha \dot{X}}{m} + \frac{\mu H_o c X}{m} = - \ddot{Z}_f + \frac{F(\theta)}{m} + \frac{g\phi^2(t)}{2} + \frac{\mu H_o}{m} b(t) \qquad \text{(III-5)}$$

IV. RESPONSE TO SINUSOIDAL FRAME DISPLACEMENT

In the absence of extraneous signals

$$b(t) = X(t) \cdot \beta AB \qquad \text{(IV-1)}$$

Therefore, from equation (III-5)

$$\ddot{X} + \frac{\alpha}{m}\dot{X} + \frac{\mu H_o}{m}(c - \beta AB)X = \ddot{Z}_f \qquad \text{(IV-2)}$$

Taking the transform of equation (IV-2) and solving for the transfer gain of the system, one obtains

$$\frac{O(s)}{Z(s)} = \frac{\beta A\, s^2}{s^2 + \frac{\alpha}{m}\, s\, \frac{\mu H_o c}{m}\left(1 - \frac{\beta AB}{c}\right)} \qquad \text{(IV-3)}$$

defining

$$\omega_o = \left\{\frac{\mu H_o c}{m}\right\}^{\frac{1}{2}} \qquad \text{(undamped resonant frequency of the unfedback system)}$$

$$\delta = \frac{\alpha}{2m\omega_o} \qquad \text{(damping factor for unfedback system)}$$

$$\gamma = \left(1 - \frac{\beta AB}{c}\right)^{\frac{1}{2}} \qquad \text{feedback parameter}$$

then

$$\frac{O(s)}{Z_f(s)} = \beta A\, \frac{s^2}{s^2 + 2\delta\omega_o s + \gamma^2 \omega_o^2} \qquad \text{(IV-4)}$$

letting $s = i\omega$ one obtains an expression for the frequency response of the system

$$\frac{O(\omega)}{Z_f(\omega)} = \beta A \frac{-\omega^2/\gamma^2\omega_o^2}{\left(1 - \frac{\omega^2}{\gamma^2\omega_o^2}\right) + i\,\frac{2\delta}{\gamma}\left(\frac{\omega}{\gamma\omega_o}\right)} \qquad \text{(IV-5)}$$

This function is plotted in Figure IV-1 for an assumed value of $\delta = 0.1$ and $0.1 \leq \gamma \leq 2.0$

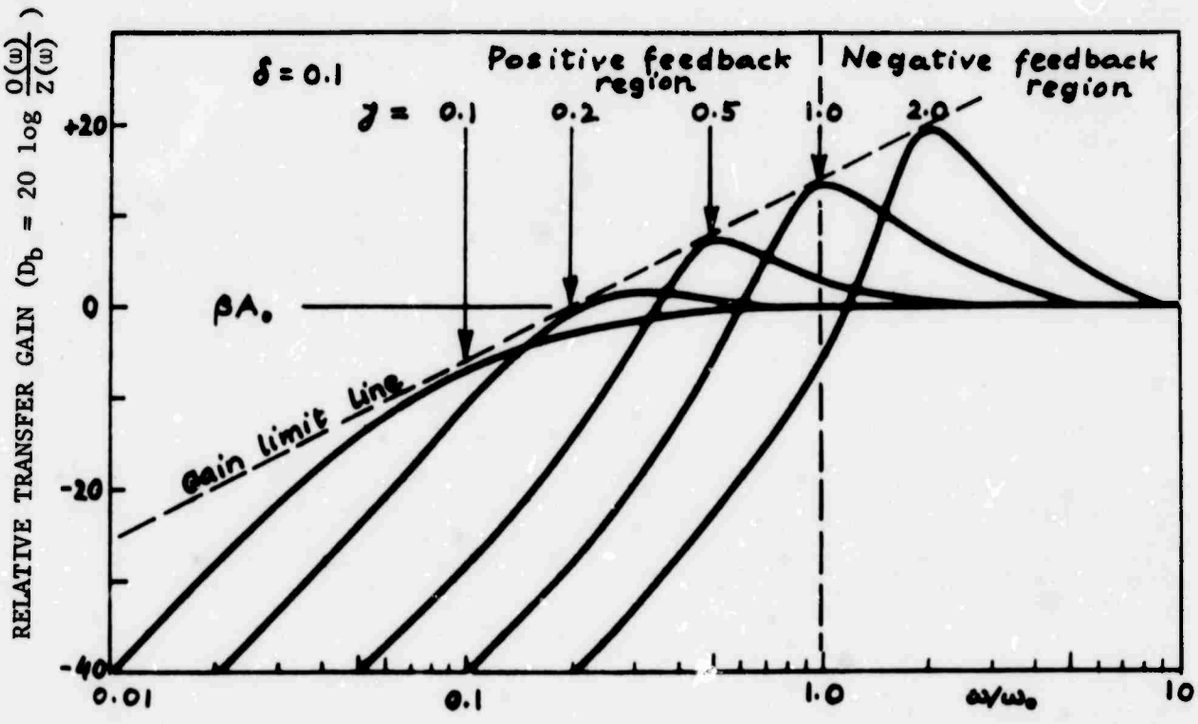

FIGURE IV-1 FEDBACK SEISMOMETER RESPONSE TO SINUSOIDAL DISPLACEMENT SIGNALS

Referring to the definition of γ, the feedback factor, it is seen that when $\gamma = 1$, there is no feedback and the system has the characteristics of a simple pendulum with damping factor δ and undamped resonance frequency ω_o. Phasing the amplifier so that it reduces γ reduces the undamped resonance frequency of the system and increases the apparent damping factor. There is a limit on loop gain in that when $\gamma = o$, the system becomes exponential rather than oscillatory, and if the gain is further increased, the system becomes exponentially divergent.

Phasing the feedback so that γ is increased beyond unity corresponds to negative feedback in that the system becomes stiffer, damping is reduced, and undamped resonant frequency is increased.

V. BROWNIAN MOTION ANALYSIS

Referring to equation (III-5) and under the assumption that $b(t) = X(t)\ \beta AB$, then with a Brownian force $F(\theta)$, one can write

$$\ddot{X} + \frac{\alpha}{m}\dot{X} + \frac{\mu H_o}{m}(c - \beta AB)\,X = \frac{F(\theta,t)}{m} \qquad \text{(V-1)}$$

$$X(s) = \frac{F(\theta),t)/m}{s^2 + \frac{\alpha}{m}s + \frac{\mu Hoc}{m}\left(1 - \frac{\beta AB}{c}\right)} \qquad \text{(V-2)}$$

$$= \frac{f(\theta,s)/m}{s^2 + 2\delta\omega_o s + \gamma^2\omega_o^2} \qquad \text{(V-3)}$$

$$O(s) = \beta AX(s) = \frac{\beta A\ f(\theta,S)/m}{s^2 + 2\delta\omega_o s + \gamma^2\omega_o^2} \qquad \text{(V-4)}$$

$$O(\theta,\omega) = \frac{\beta A\ f(\theta,\omega)/m}{-\omega^2 - 2i\delta\omega_o\omega + \gamma^2\omega_o^2} \qquad \text{(V-5)}$$

$$O(\theta,\omega) = \frac{\beta A f(\theta,\omega)}{\gamma^2\omega_o^2\, m}\ \frac{1}{\left(1 - \frac{\omega^2}{\gamma^2\omega_o^2}\right) - 2\frac{i\delta}{\gamma}\cdot\left(\frac{\omega}{\gamma\omega_o}\right)} \qquad \text{(V-6a)}$$

It will be shown that

$$f(\overline{\theta},\omega) \approx \{4\alpha k\theta\}^{\frac{1}{2}}$$

where α is the damping coefficient
k is the Boltzmann constant
θ is the absolute temperature

and that

$$O(\theta\omega) = \frac{\beta A\{4\alpha k\theta\}^{\frac{1}{2}}}{\gamma^2\omega_o^2 m} \cdot \frac{}{\left(1 - \frac{\omega^2}{\gamma^2\omega_o^2}\right) - \frac{2i\delta}{\gamma}\left(\frac{\omega}{\gamma\omega_o}\right)} \qquad \text{(V-6b)}$$

This output is plotted as a function of frequency, ω, in Figure V-1. From Figure V-1 it is obvious that as positive feedback is increased, Brownian noise voltage output is increased. It is not, however, obvious that one is loosing in signal-to-noise ratio. Signal-to-Brownian noise ratio can be calculated by dividing equation (IV-5) by equation (V-6) one obtains

$$\frac{S}{N} = \frac{O(\omega)}{O(\theta,\omega)} = \frac{\beta A \dfrac{\dfrac{-\omega^2}{\gamma^2\omega_o^2} Z_f(\omega)}{\left(1 - \dfrac{\omega^2}{\gamma\omega_o^2}\right) + \dfrac{i2\delta}{\gamma}\left(\dfrac{\omega}{\gamma\omega_o}\right)}}{\dfrac{\beta A f(\theta,\omega)}{m\gamma^2\omega_o^2} \dfrac{1}{\left(1 - \dfrac{\omega^2}{\gamma\omega_o^2}\right) + \dfrac{2i\delta}{\gamma}\left(\dfrac{\omega}{\gamma\omega_o}\right)}} = \frac{-m\omega^2 Z_f(\omega)}{\{2\alpha k\theta\}^{\frac{1}{2}}} \qquad \text{(V-7)}$$

From this relationship, one concludes that the signal-to-Brownian noise ratio is unaffected by the adjustment of the feedback parameter. It is a function of frequency (ω), temperature (θ), the unfedback mechanical damping constant α, and input signal spectrum level $Z(\omega)$.

The seismometer designer can control and maximize signal-to-Brownian noise ratio by minimizing α and θ and maximizing m.

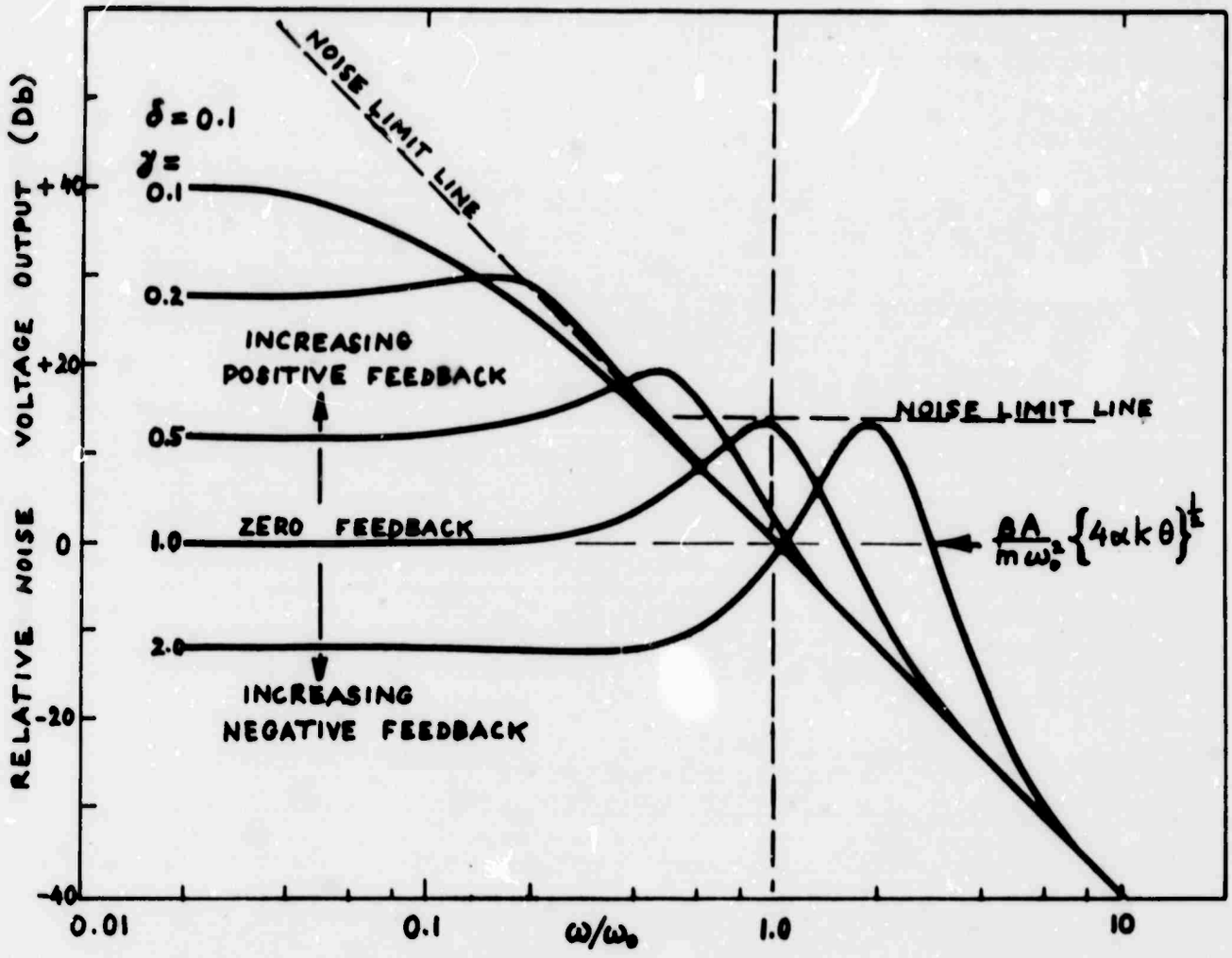

FIGURE V-1 RELATIVE OUTPUT BROWNIAN NOISE VOLTAGE AS A FUNCTION OF FREQUENCY WITH FEEDBACK FACTOR γ AS A PARAMETER

VI. DERIVATION OF THE BROWNIAN FORCE SPECTRAL DENSITY

Consider a simple spring mass system characterized by the constants m, α and k so that

$$m\ddot{y} + \alpha\dot{y} + ky = B(t) \qquad \text{(VI-1)}$$

Taking the transform of this equation, one obtains an expression for the transform of the displacement of the mass m in terms of the transform of the applied force, that is:

$$y(s) = \frac{b(s)}{m} \cdot \frac{1}{s^2 + \frac{\alpha s}{m} + \frac{k}{m}} \qquad \text{(VI-2)}$$

Letting $s = i\omega$ and solving for the squared magnitude of the quantity on the right, one obtains an expression for the power spectral density of $|y^2(f)|$ under the condition that $B(\tau)$ is a random, stationary ergodic function[1] that is

$$\frac{d}{df}\left|y^2(f)\right| df = \frac{1}{2\pi}\frac{d}{d\omega}\left|y^2(\omega)\right| d\omega \qquad \text{(VI-3)}$$

$$\frac{d}{df}\left|y^2(f)\right| df = \frac{1}{2\pi m^2}\left\{\frac{d}{d\omega} b^2(\omega)\, d\omega\right\} \frac{1}{\left(\frac{k}{m} - \omega^2 + \frac{i\alpha}{m}\right)\left(\frac{k}{m} - \omega^2 - \frac{i\alpha}{m}\right)}$$

---

(1) Measurement and Analysis of Random Data, Bendat and Piersol, John Wiley & Sons, New York, N. Y. 1966. Chapter 1.

Formally integrating equation (3), one obtains

$$\overline{y^2} = \int_0^\infty \frac{d}{df}\, y^2(f)\,df = \frac{1}{2\pi m^2} \int_0^\infty \frac{d}{d\omega}\, b^2(\omega)\, \frac{d\omega}{\left(\frac{k}{m} - \omega^2 + i\alpha\right)\left(\frac{k}{m} - \omega^2 - i\alpha\right)} \qquad \text{(VI-4)}$$

$$\overline{y^2} = \frac{1}{4\pi m^2} \int_{-\infty}^{\infty} \frac{d}{d\omega}\, b^2(\omega) \cdot \frac{d\omega}{\left[\omega - \frac{i\alpha}{2m} + \frac{1}{2}\left(\frac{4k}{m} - \frac{\alpha^2}{m^2}\right)^{\frac{1}{2}}\right]\left[\omega + \frac{i\alpha}{2m} + \frac{1}{2}\left(\frac{4k}{m} - \frac{\alpha^2}{m^2}\right)\right]\left[\omega - \frac{i\alpha}{2m} - \frac{1}{2}\left(\frac{4k}{m} - \frac{\alpha^2}{m^2}\right)\right]\left[\omega + \frac{i\alpha}{2m} - \frac{1}{2}\left(\frac{4k}{m} - \frac{\alpha^2}{m^2}\right)\right]^{\frac{1}{2}}} \qquad \text{(VI-5)}$$

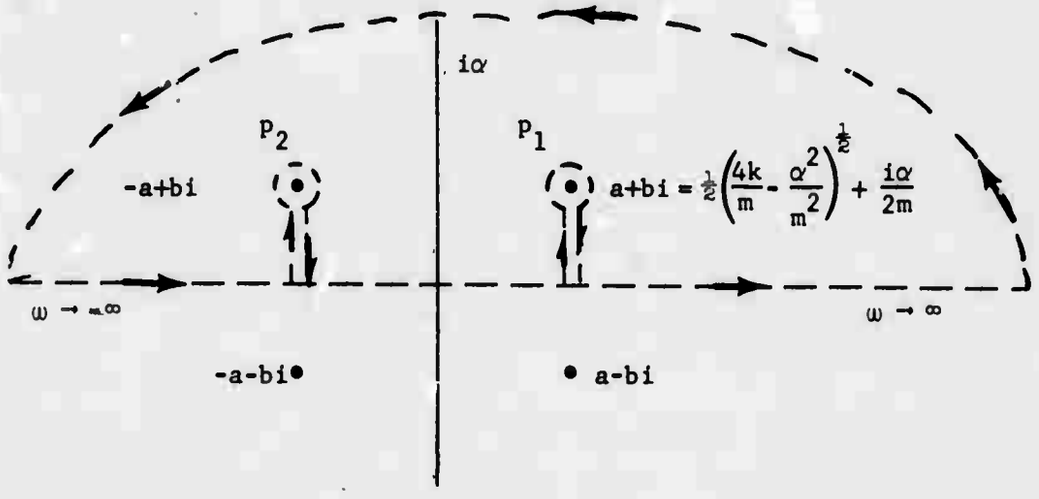

Since $\frac{d}{d\omega}\, b^2(\omega)$ must be a positive definite real quantity

$$\overline{y^2} = \frac{2\pi i}{4\pi m^2} \sum R = \frac{i}{2}\left\{R_1 + R_2\right\} \qquad \text{(VI-6)}$$

$$R_1 = \frac{\frac{d}{d\omega}\, f_b^2\left[\frac{1}{2}\left(\frac{4k}{m} - \frac{\alpha^2}{m^2}\right)^{\frac{1}{2}} + \frac{i\alpha}{2m}\right]}{\left(\frac{4k}{m} - \frac{\alpha^2}{m^2}\right)^{\frac{1}{2}}\left[\frac{i\alpha}{m} + \left(\frac{4k}{m} - \frac{\alpha^2}{m^2}\right)^{\frac{1}{2}}\right]\left(\frac{i\alpha}{m}\right)}$$

$$R_2 = \frac{\frac{d}{d\omega} f_b^2 \left[-\frac{1}{2} \left(\frac{4k}{m} - \frac{\alpha^2}{m^2} \right)^{\frac{1}{2}} + \frac{i\alpha}{2m} \right]}{\frac{i\alpha}{m} (-) \left(\frac{4k}{m} - \frac{\alpha^2}{m^2} \right)^{\frac{1}{2}} \left[\frac{i\alpha}{m} - \frac{4k}{m} - \frac{\alpha^2}{m^2} \right]^{\frac{1}{2}}}$$

Since $b^2(\omega)$ is a positive real quantity

$$\frac{d}{d\omega} b^2 \left(\frac{1}{2} \left[\frac{4k}{m} - \frac{\alpha^2}{m^2} \right]^{\frac{1}{2}} + \frac{i\alpha}{2m} \right) = \frac{d}{d\omega} b^2 \left(\frac{1}{2} \left[\frac{4k}{m} - \frac{\alpha^2}{m^2} \right]^{\frac{1}{2}} - \frac{i\alpha}{2m} \right) \qquad \text{(VI-7)}$$

then

$$\overline{y^2} = \frac{i}{2m^2} \cdot \frac{d}{d\omega} b^2 \left[\frac{1}{2} \left(\frac{4k}{m} - \frac{\alpha^2}{m^2} \right)^{\frac{1}{2}} + \frac{i\alpha}{2m} \right] \cdot \frac{1}{\frac{i\alpha}{m} \left(\frac{4k}{m} - \frac{\alpha^2}{m^2} \right)^{\frac{1}{2}}} \left\{ \frac{1}{\frac{i\alpha}{m} + \left(\frac{4k}{m} - \frac{\alpha^2}{m^2} \right)^{\frac{1}{2}}} - \frac{1}{\frac{i\alpha}{m} - \left(\frac{4k}{m} - \frac{\alpha^2}{m^2} \right)^{\frac{1}{2}}} \right\} \qquad \text{(VI-8)}$$

$$\overline{y^2} = \frac{d}{d\omega} b^2 \left(\frac{1}{2} \left[\frac{4k}{m} - \frac{\alpha^2}{m^2} \right]^{\frac{1}{2}} + \frac{i\alpha}{2m} \right) \cdot \frac{1}{2\alpha m} \left\{ \frac{-2 \left(\frac{4k}{m} - \frac{\alpha^2}{m^2} \right)^{\frac{1}{2}}}{-\frac{\alpha^2}{m^2} - \frac{4k}{m} + \frac{\alpha^2}{m^2}} \cdot \frac{1}{\left(\frac{4k}{m} - \frac{\alpha^2}{m^2} \right)^{\frac{1}{2}}} \right\} \qquad \text{(VI-9)}$$

$$\overline{y^2} = \frac{d}{d\omega} b^2 \left(\frac{1}{2} \left[\frac{4k}{m} - \frac{\alpha^2}{m^2} \right]^{\frac{1}{2}} + \frac{i\alpha}{2m} \right) \cdot \frac{1}{4\alpha k} \qquad \text{(VI-10)}$$

However,

$$\frac{1}{2} k \overline{y^2} = \frac{1}{2} k \theta \qquad \text{(VI-11)}$$

where k is the Boltzmann constant

θ is the absolute temperature

Therefore,

$$\frac{d}{d\omega} b^2 \left(\frac{1}{2} \left[\frac{4k}{m} - \frac{\alpha^2}{m^2} \right]^{\frac{1}{2}} + \frac{i\alpha}{2m} \right) = 4\alpha k \theta \qquad \text{(VI-12)}$$

This implies that $d/d\omega\ f_b^2$ is a function of α and Θ only independent of k, m or ω. This then states that the Brownian force power density spectrum is a constant for fixed damping coefficient α and for fixed temperature Θ and this is given by

$$\boxed{\frac{d}{df}\, b^2\ (f) = 4\alpha k\Theta} \qquad \text{(VI-13)}$$

and

$$b(f) = \{4\alpha k\Theta\}^{\frac{1}{2}} \qquad \text{(VI-14)}$$

VII. TILT SIGNALS

Referring to equation (III-5) a generalized force balance equation can be written in the form

$$\ddot{X} + \frac{\alpha \dot{X}}{m} + \frac{\mu H_o c}{m} X = \frac{F(t)}{m} + \frac{\mu H_o}{m} b(t) \qquad \text{(VII-1)}$$

for tilt signals,

$$F(t) = \frac{mg}{2} \phi(t)^2 \qquad \text{(VII-2)}$$

given that

$$b(t) = X(t)\, \beta A B \qquad \text{(VII-3)}$$

$$O(t) = \beta A\, X(t) \qquad \text{(VII-4)}$$

then

$$(\delta^2 + 2\delta\omega_o\delta + \gamma^2 \omega_o^2)X(\delta) = f(\delta) \qquad \text{(VII-5)}$$

$$O(\delta) = \frac{\beta A\, f(\delta)}{(\delta^2 + 2\delta\, \omega_o\delta + \gamma^2\, \omega_o^2)} \qquad \text{(VII-6)}$$

$$O(\omega) = \frac{\beta A\, g\phi^2(\omega/2)}{2\gamma^2\, \omega_o^2} \cdot \frac{1}{\left(1 - \frac{\omega^2}{\gamma^2 \omega_o^2}\right) - \frac{2i\delta}{\gamma}\left(\frac{\omega}{\gamma\omega_o}\right)} \qquad \text{(VII-7)}$$

This equation is of the same form as equation (VI-6a) and will therefore lead to the same conclusions, i.e., signal-to-tilt noise ratios are unaffected by feedback.

Tilt Frequency Doubling

An interesting aspect of the instrument's tilt sensitivity is the frequency doubling plus dc offset that occurs with a periodic tilt signal.

If one assumes a tilt of the form

$$\phi(t) = \phi_o \sin \frac{\omega t}{2} \qquad \text{(VII-8)}$$

then

$$F(t) = \frac{mg}{2} \phi^2(t) = \frac{mg}{2} \phi_o^2 \sin^2 \frac{\omega t}{2} \qquad \text{(VII-9)}$$

$$F(t) = \frac{mg}{4} \phi_o^2 \{1 - \cos \omega t\} \qquad \text{(VII-10)}$$

Therefore, for a periodic tilt at frequency $\omega/2$ one gets a forcing function that has a dc component plus a periodic component at frequency ω. The dc term is given by

$$O(o) = \frac{\beta A\, g\, \phi_o^2}{2\gamma^2\, \omega_o^2} \qquad \text{(VII-11)}$$

VIII. ELECTRONIC NOISE

Referring to Figure II-1, it can be seen that

$$O(t) = (\beta X(t) + \eta(t))A \qquad \text{(VIII-1)}$$

$$O(s) = \{\beta X(s) + \eta(s)\}A$$

$$b(t) = BO(t) \qquad \text{(VIII-2)}$$

$$F_b = \mu H_o b(t) = \mu H_o B\, O(t) \qquad \text{(VIII-3)}$$

$$\ddot{X} + \frac{\alpha X}{m} + \frac{\mu H_o c X}{m} = \frac{\mu H_o BA}{m}(\beta X(t) + \eta(t)) \qquad \text{(VIII-4)}$$

$$X\left[s^2 + \frac{\alpha s}{m} + \frac{\mu H_o c}{m}\left(1 - \frac{\beta AB}{c}\right)\right] = \frac{\mu H_o BA}{m}\,\eta(s) \qquad \text{(VIII-5)}$$

$$X(s) = \frac{\eta(s)\,\frac{\mu H_o BA}{m}}{s^2 + \frac{\alpha}{m}s + \frac{\mu H_o c}{m}\left(1 - \frac{\beta AB}{c}\right)} \qquad \text{(VIII-6)}$$

$$\frac{O(s)}{\eta(s)} = \frac{\left(\frac{\mu H_o \beta B}{m} + 1\right)A}{s^2 + \frac{\alpha}{m}s + \frac{\mu H_o c}{m}\left(1 - \frac{\beta AB}{c}\right)} \qquad \text{(VIII-7)}$$

$$\frac{\theta(\omega)}{\eta(\omega)} = \frac{\left(\frac{\mu H_o}{m}\beta B + 1\right) A}{-\omega^2 + 2i\delta\,\omega_o\omega + \gamma^2\,\omega_o^2} = \frac{1 + \frac{A\beta\omega_o}{c}}{\gamma^2\omega_o^2\left\{\left[1 - \left(\frac{\omega}{\gamma\omega_o}\right)^2\right] + \frac{2i\delta}{\delta}\left(\frac{\omega}{\gamma\omega_o}\right)\right.} \qquad \text{(VIII-8)}$$

Here again, one sees the output voltage due to noise input increases as $\gamma \to 0$ (i.e., positive feedback): however, the signal-to-noise ratio will again be independent of the amount and type of feedback used.

IX. ROOT LOCUS AND TRANSIENT RESPONSE

Referring to equation (IV-3)

$$\frac{O_1(s)}{Z_f(s)} = \beta A \frac{s^2}{s^2 + \frac{\alpha}{m} s + \gamma^2 \frac{k}{m}} \qquad \text{(IX-1)}$$

Upon substitution of $\delta_o = \frac{\alpha}{2m\,\omega_o}$, $\omega_o^2 = \frac{k}{m}$, one obtains

$$\frac{O_1(s)}{Z_f(s)} = \beta A \frac{s^2}{s^2 + 2\delta_o\,\omega_o s + \gamma^2\,\omega_o^2} \qquad \text{(IX-2)}$$

The denominator can be factored in that

$$s = \frac{-2\delta_o\omega_o \pm \left\{4\delta_o^2\,\omega_o^2 - 4\gamma^2\omega_o^2\right\}}{s}$$

$$s = \omega_o\left[-\delta_o \pm \left\{\delta_o^2 - \gamma^2\right\}^{\frac{1}{2}}\right]$$

$$\frac{O_1(s)}{Z_f(s)} = \beta A \frac{s^2}{\left[s+\omega_o\delta_o + \left\{\delta_o^2 - \gamma^2\right\}^{\frac{1}{2}}\right]\left[s + \delta_o - \left\{\delta_o^2 - \gamma^2\right\}^{\frac{1}{2}}\right]} \qquad \text{(IX-3)}$$

The function in (IX-3) will have poles at

$$s = \omega_o\left[-\delta_o \pm \left\{\delta_o^2 - \gamma^2\right\}^{\frac{1}{2}}\right]$$

There is a series of points of interest:

CASE I $\gamma^2 < 0 \Rightarrow \left\{\delta_o^2 - \gamma^2\right\}^{\frac{1}{2}}$ real and $> \delta$.

The solution is therefore made up of exponentials of the form

$$e^{-[2\delta_o + \epsilon\delta_o]t} \quad \text{and} \quad e^{+\epsilon\delta_o t}$$

The system therefore is unstable, due to the positive exponential term.

CASE II $\gamma^2 = 0$ Under this condition the function has a pole at the origin and at $-2\delta_o$, solutions will contain a single solution of the form

$$e^{-2\delta_o t}$$

The system is stable and approaches equilibrium exponentially.

CASE III $0 < \gamma^2 < \delta_o^2 \Rightarrow \left\{\delta_o^2 - \gamma^2\right\}^{\frac{1}{2}}$ real and $< \delta_o$

The solution is therefore made up of exponentials of the form

$$e^{-[2\delta_o - \epsilon\delta_o]t} \quad \text{and} \quad e^{-\epsilon\delta_o t}$$

The system is therefore stable in that it approaches equilibrium exponentially.

CASE IV $\gamma_o^2 = \delta_o^2$, the system has a pole of order 2 at $-\delta_o$ and solutions will be of the form

$$1 - t\, e^{-\delta_o t}$$

The system is stable but now approaches equilibrium after one zero crossing.

CASE V $\gamma_o > \delta_o^2$ The system has poles at

$$s = -\omega_o \delta_o \pm i\omega_o \left\{ \gamma^2 - \delta_o^2 \right\}^{\frac{1}{2}}$$

Solutions will be of the form

$$e^{-\gamma_o t} \sin \omega_o \left\{ \gamma^2 - \delta_o^2 \right\}^{\frac{1}{2}} t$$

The system is stable and will approach equilibrium with a damped sine wave response

The root locus can now be sketched in the complex s plane as shown:

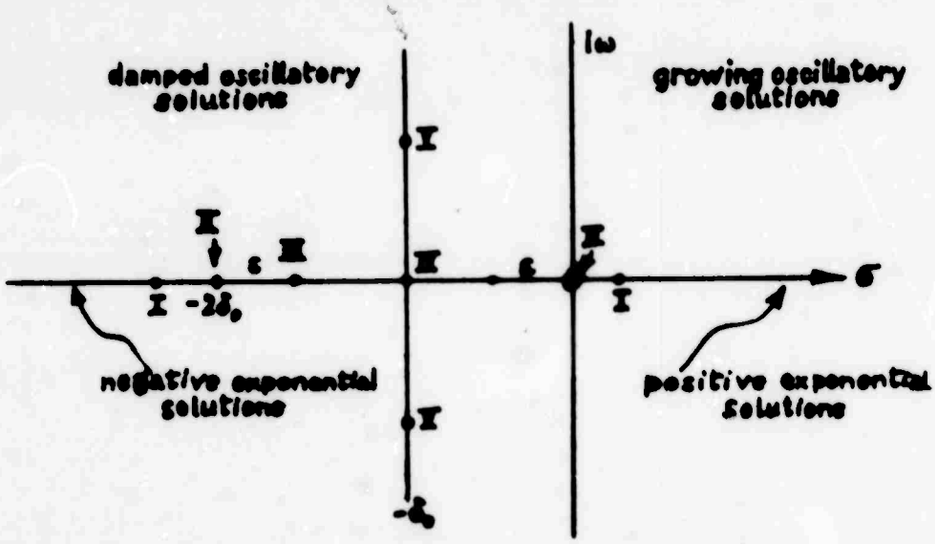

FIGURE IX-1 ROOT LOCUS FOR TRANSFER GAIN

For a step input in $Z_f(t)$ one would obtain Figure IX-2:

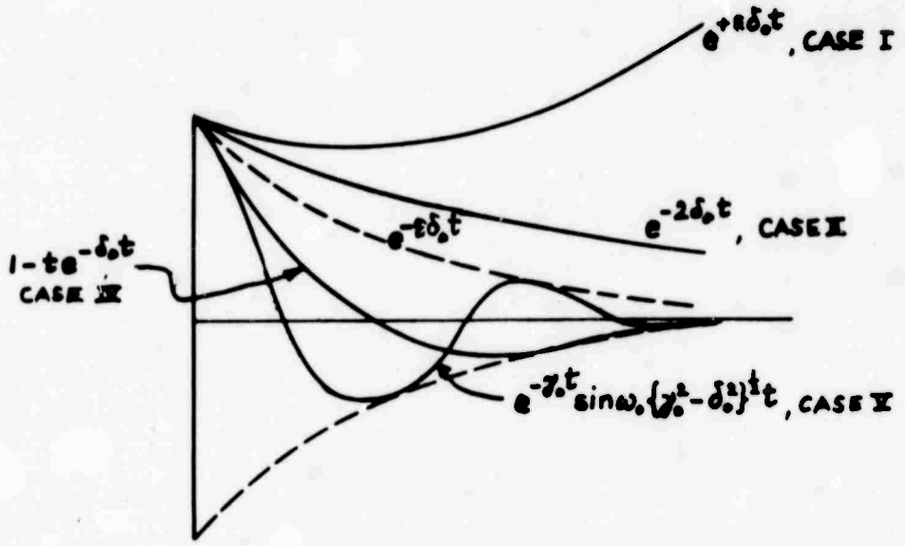

FIGURE IX-2 FEDBACK SEISMOMETER TRANSIENT RESPONSE FOR STEP MOVEMENT OF FRAME

X. DRIFT

Substituting equation (III-2) into equation (II-1) in the absence of ground motion, Brownian, tilt and electronic noise, one obtains

$$m\ddot{X} + \alpha\dot{X} = \mu H_o \left[a + b(t) - c \cdot X(t)\right] - mg$$

Now let us assume that H_o, a or c are slowly varying functions of time, then as $\omega \to 0$

$$a + b(t) - c\,X(t) = \frac{mg}{\mu H_o} \qquad \text{(X-1)}$$

However, from equation IV-1 $b(t) = \beta AB\, X(t)$

$$a + (\beta AB - c)\, X(t) = \frac{mg}{\mu H_o} \qquad \text{(X-2)}$$

$$X(t) = \left\{ \frac{mg}{\mu H_o} - a \right\} \frac{1}{\beta AB - c} \qquad \text{(X-3)}$$

To assure that $X(t) \to 0$ at dc ($\omega \to o$) it is necessary to have $\beta AB \to \infty$ as $w \to o$. This implies very strong negative feedback at low frequencies.

If we compare the instrument drift with and without feedback, we have

$$\left.\frac{X(t) \text{ feedback}}{X(t) \text{ open loop}}\right|_{\omega \to o} = \frac{\left\{ \frac{mg}{\mu H_o} - a \right\} \frac{1}{c - \beta AB}}{\left\{ \frac{mg}{\mu H_o} - a \right\} \frac{1}{c}} = \frac{c}{c - \beta AB} \qquad \text{(X.4)}$$

$$\left|\frac{X(t)\ \text{feedback}}{X(t)\ \text{open loop}}\right|_{\omega \to o} = \frac{1}{1 - \frac{\beta AB}{c}} = \frac{1}{\gamma\ (\omega \to o)} \qquad (X\text{-}5)$$

The drift of the instrument is therefore reduced by a factor of $\frac{1}{\gamma_{(\omega \to o)}}$.

XI. FEEDBACK CIRCUIT DESIGN A

Consider a circuit of the type shown in Figure XI-1.

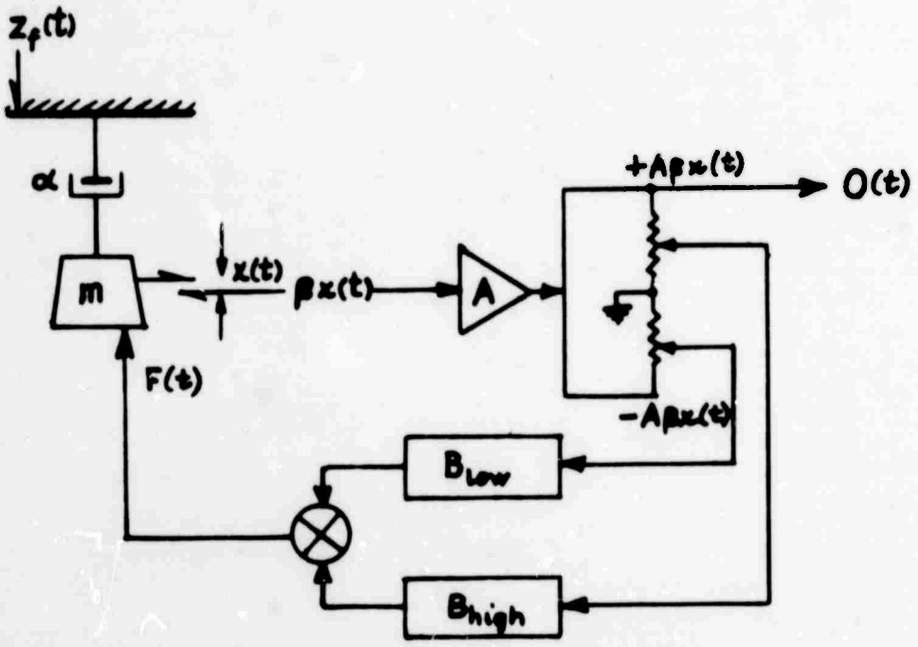

FIGURE XI-1. STABILIZED FEDBACK VERTICAL SEISMOMETER

In the circuit sketched one feeds back negatively at low frequencies and positively at high frequencies. A sketch of the Bode diagram for this system is shown in Figure XI-2.

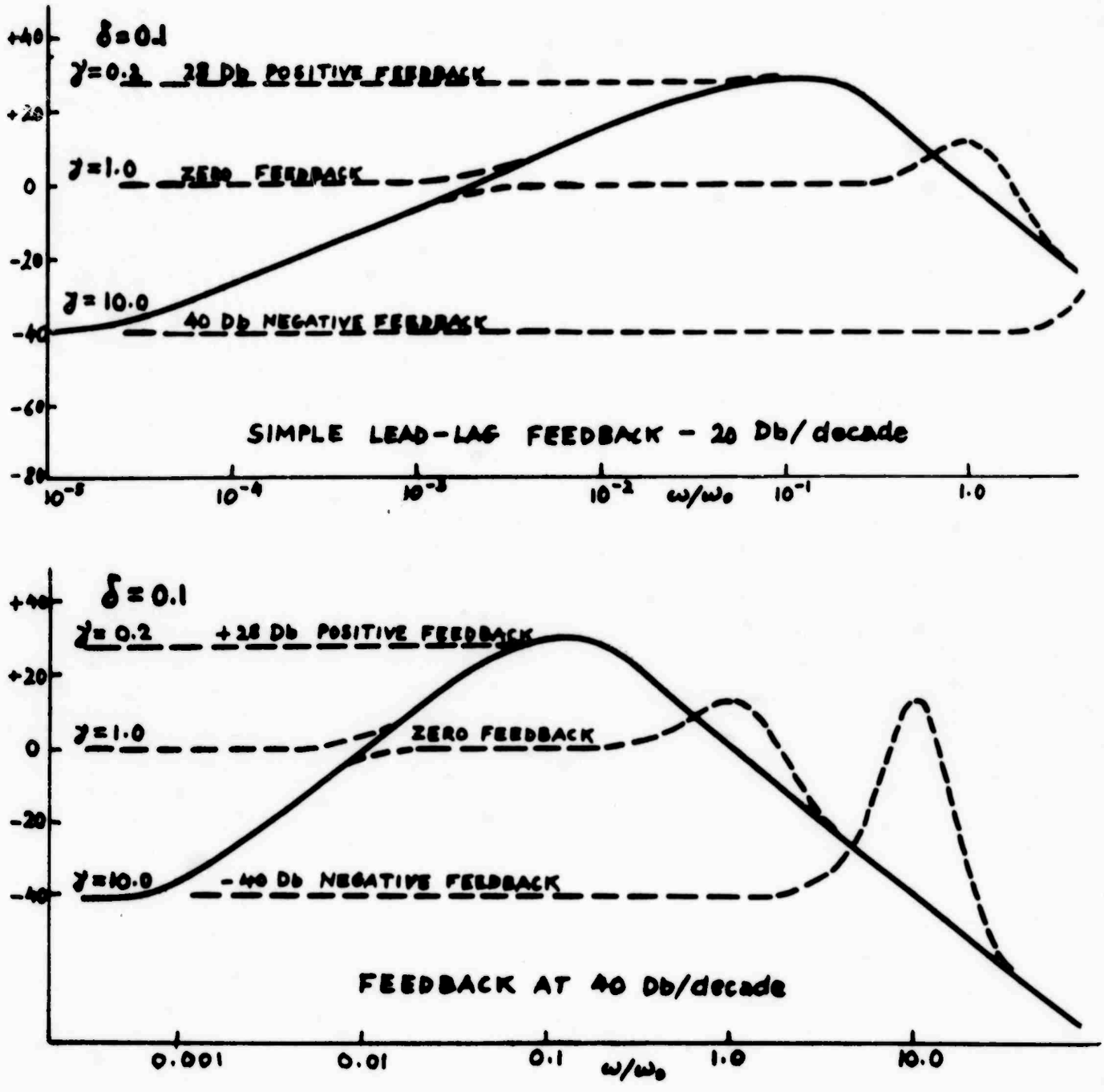

FIGURE XI-2. BODE DIAGRAM FOR STABILIZED SEISMOMETER

The upper diagram in Figure XI-2 corresponds to the case where B_{low} is a simple low-pass filter with a corner frequency at $2 \times 10^{-5}\ \omega_o$, and B_{high} is a high pass filter with a corner frequency at $5 \times 10^{-2}\ \omega_o$. The lower diagram indicates the change in response if the filters cut off at the rate of 40 db/decade rather than 20 db/decade. The diagrams are for the overall input-output frequency response.

It should be emphasized that in this design the overall fedback dynamic response of the mass is equivalent to that of a critically damped simple pendulum with undamped resonance frequency equal to 0.2 times the undamped resonance frequency of the unfedback system.

In this design, the mass moves with respect to the frame.

XII. FEEDBACK CIRCUIT DESIGN B

Because of dynamic range, linearity, temperature, stability and gain constancy considerations, Martin Cohen suggests that the system should be negatively fedback over the entire operating range so that the seismic mass is constrained not to move over the frequency range of interest and further, that only a portion of the shaping be done within the loop with final shaping and gain adjustment being accomplished by post-amplification and filtering. A design of this type is sketched in Figure XII-1.

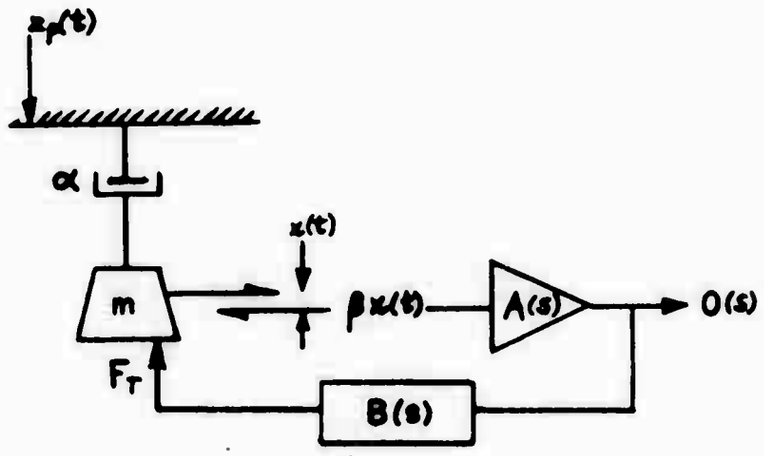

FIGURE XII-1. NEGATIVELY FEDBACK VERTICAL SEISMOMETER

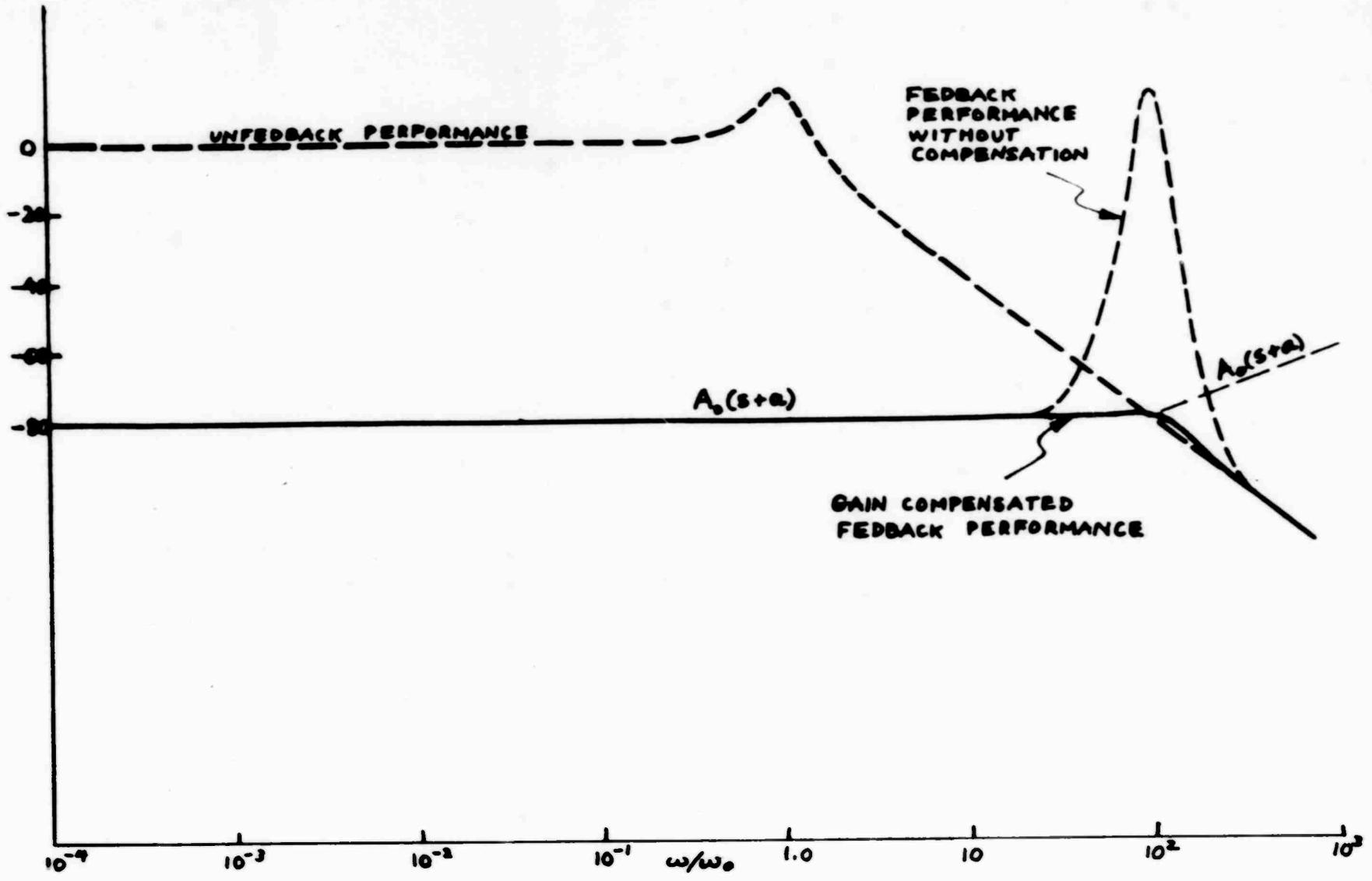

FIGURE XII-2. ACCELERATION RESPONSE OF GAIN COMPENSATED NEGATIVELY FEDBACK SEISMOMETER

The device sketched will have an acceleration response of the form

$$\frac{O(s)}{s^2 Z_f(s)} = \frac{\beta A(s)}{s^2 + \frac{\alpha}{m} s + \frac{\mu H_o c}{m}\left(1 - \frac{\beta A(s) B(s)}{c}\right)} \qquad \text{(XII-1)}$$

If in the frequency range of interest $A(s) = A_o \{S + a\}$, then

$$\frac{O(s)}{s^2 Z_f(s)} = \frac{\beta A_o \{s + a\}}{s^2 + \left(\frac{\alpha}{m} - \frac{\beta A_o B(s)}{a} \frac{\mu H_o c}{m} s\right) + \frac{\mu H_o c}{m}\left(1 + \frac{\beta A_o B}{c} a\right)} \qquad \text{(XII-2)}$$

$$\frac{O(s)}{s^2 Z_f(s)} = \frac{\beta A_o \{s + a\}}{s^2 + \left(2\delta\omega_o + \frac{\gamma^2\omega_o^2 - 1}{a}\right) s + \gamma^2\omega_o^2} \qquad \text{(XII-3)}$$

Since the constant a can be chosen, the damping at the fedback resonance can be adjusted to obtain a critically damped system. The Bode diagram for this system is shown in Figure XII-2. As seen from this diagram, the acceleration response over the range of frequencies of interest is flat.

The transfer gain for acceleration in this region is given by

$$\frac{O(s)}{s^2 Z_f(s)} = \frac{\beta Aa}{\gamma^2\omega_o^2} = \frac{\beta Aa}{\frac{\mu H_o c}{m}\left(1 + \frac{\beta A_o Ba}{c}\right)} \approx \frac{1}{\frac{\mu H_o}{m} \cdot B} \qquad \text{(XII-4)}$$

and therefore a function of the force constant of the feedback only.

UNCLASSIFIED

Security Classification

DOCUMENT CONTROL DATA - R & D

(Security classification of title, body of abstract and indexing annotation must be entered when the overall report is classified)

1. ORIGINATING ACTIVITY (Corporate author)

Arthur D. Little, Inc.
Research and Development Division
Cambridge, Massachusetts 02140

2a. REPORT SECURITY CLASSIFICATION

UNCLASSIFIED

2b. GROUP

3. REPORT TITLE

DEVELOPMENT OF A THREE-AXIS LONG-PERIOD SEISMOGRAPH

4. DESCRIPTIVE NOTES (Type of report and inclusive dates)

Scientific Interim

5. AUTHOR(S) (First name, middle initial, last name)

Ivan Simon

6. REPORT DATE	7a. TOTAL NO. OF PAGES	7b. NO. OF REFS
31 May 1968	36	0

8a. CONTRACT OR GRANT NO.	9a. ORIGINATOR'S REPORT NUMBER(S)
AF44620-67-C-0107	
b. PROJECT NO. 9741	
c.	9b. OTHER REPORT NO(S) (Any other numbers that may be assigned this report) AFOSR 68-2152
d. 6250601R	

10. DISTRIBUTION STATEMENT

1. This document has been approved for public release and sale; its distribution is unlimited.

11. SUPPLEMENTARY NOTES	12. SPONSORING MILITARY ACTIVITY
Tech, Other	Air Force Office of Scientific Research 1400 Wilson Blvd. (SRPG) Arlington, Virginia 22209

13. ABSTRACT

Development of a three-component long-period borehole seismometer of small diameter /5-1/2 inches O.D./ is described. The feasibility of the magnetic suspension principle has been demonstrated and several instruments have been constructed and tested in the laboratory.

DD FORM 1 NOV 65 1473

UNCLASSIFIED

Security Classification